SI Appendix

"Cell size and growth regulation in the *Arabidopsis thaliana* apical stem cell niche"

Authors: Lisa Willis[a,b,1], Yassin Refahi[a,1], Raymond Wightman[a], Benoit Landrein[a], José Teles[a], Kerwyn Casey Huang[b,c], Elliot M Meyerowitz[a,d], Henrik Jönsson[a,e,f,2]

[1]Equal contributions

Author affiliations: [a]The Sainsbury Laboratory, Cambridge University, Bateman Street, Cambridge, CB2 1LR, UK

[b]Department of Bioengineering, Stanford University, Stanford, CA 94305, USA

[c]Department of Microbiology and Immunology, Stanford University School of Medicine, Stanford, CA 94305, USA

[d]Howard Hughes Medical Institute and Division of Biology and Biological Engineering 156-29, California Institute of Technology, Pasadena, CA 91125, USA

[e]Computational Biology and Biological Physics, Lund University, Sölvegatan 14A, 223 62 Lund, Sweden

[f]Department of Applied Mathematics and Theoretical Physics, Centre for Mathematical Sciences, Cambridge University, Wilberforce Road, Cambridge, CB3 0DZ, UK

[2]**Corresponding author**: Henrik Jönsson, The Sainsbury Laboratory, Cambridge University, Bateman Street, Cambridge, CB2 1LR, UK. Tel: +44(0)1223 761100.

Email: Henrik.Jonsson@slcu.cam.ac.uk

Keywords: cell size, cell growth, cell cycle, homeostasis, plant stem cells

Supplementary Materials and Methods

Pipeline for 4D cellular quantification and tracking using MARS/ALT. Confocal *z*-stacks were processed in a semi-automated pipeline. The ImageJ registration plugin StackReg (61) using the translation transformation was applied to each stack, to correct for misalignments between consecutive *z*-slices due to stage adjustments. Any *z*-slices that contained horizontal shifts due to sudden large vibrations or stage movements during *z*-stack acquisition were identified, then automatically replaced with the closest *z*-slice that had no horizontal shift (~1-5% slices); this process helped to eliminate segmentation errors. A potential major source of cellular quantitation error is the upward movement of the plantlet during *z*-stack acquisition due to stem elongation: for most time-points, the plantlet gained height in the *z*-direction at a velocity comparable to that of the confocal scan-head, which resulted in an artificially stretched SAM by a mean factor of ~1.3, with a maximum stretching factor of ~2.3 (*SI Appendix*, Fig. S24; Table S10). To correct this artifact, *z*-slices of the low-*z*-resolution stack (*z*-step = 5-6 μm), which was not artificially stretched and which was acquired immediately after the high z-resolution stack (*z*-step = 0.25 μm), were matched with corresponding *z*-slices of the high-*z*-resolution *z*-stack to compute and correct for the stretching.

To remove noise from the processed *z*-stacks, we applied a Gaussian filter and an alternative-sequential filter (ASF). These filtered z-stacks were segmented (independently of z-stacks at other time-points) using a 3D watershed algorithm from MARS [1]. The watershed seeds were determined using the h-minima operator, which computes local minima regions in the filtered *z*-stacks. For a visual assessment of segmentation quality, cell boundary stacks were computed from the segmentations using a 3D Laplace filter from the SciPy library then the cell boundary

stacks and processed z-stacks were merged with different colors into a single stack in ImageJ. This merged stack was visually inspected for segmentation errors (Movies S5-S6). In case of a segmentation error (over-segmentation, under-segmentation, missed cell, or shape error), we changed the parameters of the Gaussian and ASF filters as well as the h-minima parameter of the segmentation algorithm to optimize segmentation of the L1 layer. In the optimal segmentations, the lower layers of the central and peripheral zones were also mostly error free.

For this exposition, we define I_t and $I_{t+\Delta t}$ as the processed z-stacks from two consecutive confocal acquisitions, and S_t and $S_{t+\Delta t}$ as the corresponding optimal segmentations. To track cell lineages between S_t and $S_{t+\Delta t}$, we first computed the affine transformation that linearly registered I_t onto $I_{t+\Delta t}$ using the block-matching framework (62-64). The affine transformation was then used to initialize the block-matching algorithm to compute the non-linear transformation $T_{I_t \leftarrow I_{t+\Delta t}}$, a vector field that was used for the final registration between segmentations S_t and $S_{t+\Delta t}$. For a visual assessment of the quality of registration, we imported the reference image $I_{t+\Delta t}$ and the registered floating image $I_t \circ T_{I_t \leftarrow I_{t+\Delta t}}$into ImageJ and merged them with different colors (red: $I_{t+\Delta t}$, green: $I_t \circ T_{I_t \leftarrow I_{t+\Delta t}}$) into a single image (Movie S7). Registration quality was then visually verified by inspecting this merged image in 3D. Registration was perfect for 138/140 pairs of consecutive images, reflecting the fact that the image-acquisition frequency ($\Delta t = 4\ \mathrm{h}$) had sufficiently high temporal resolution. To compute mother-daughter cell pairings between consecutive time-points, the non-linear registration was applied to S_t (i.e. $S_t \circ T_{I_t \leftarrow I_{t+\Delta t}}$), then ALT (60) was used to compute the optimal mother-daughter pairing between $S_t \circ T_{I_t \leftarrow I_{t+\Delta t}}$ and $S_{t+\Delta t}$. When ALT failed (2/140 pairs of consecutive time-points), we manually paired mother and daughter cells. The optimal pairing was then used to generate color maps in which the mother

and daughter cells had the same color code. These color maps were used to visualize the segmentations and visually verify computed lineages (Fig. 1A).

Volume and surface area quantification and validation. In the 3D segmented *z*-stacks, voxels belonging to the same cell were marked by the same label. Cell volumes were computed by counting the number of voxels with the same label, and multiplying this count by the given voxel volume. Accurate estimation of cell surface area was more challenging (65-67). To extract cell surfaces, we used the marching cubes algorithm from the Visualization Toolkit (VTK) version 5.8 (68), which generated triangular meshes of cell surfaces. Cell surface area was computed after decimating the mesh (while preserving cell-cell topology), and then Laplacian smoothing the mesh using algorithms from VTK v. 5.8. To assess the accuracy of surface area quantification, we generated digitized synthetic spheres, cylinders, and cubes of different dimensions on a 3D grid of 0.25×0.25×0.25 μm^3 voxels to match the resolution of our confocal *z*-stacks. For different shapes of the same volume as the average cell of the meristem (~160 μm^3), the error was <5%.

Nuclear volume quantification. The nuclear-localized pCLV3::dsRED-N7 reporter was used to segment L1 nuclei in the center of SAMs #2-6. Prior to segmentation, the pCLV3::dsRED-N7 channels of all confocal *z*-stacks were deconvolved to remove fluorescence artifacts due to the confocal microscope's point-spread function (PSF). Deconvolution was performed using Huygens software version 15.05 (Scientific Volume Imaging, Hilversum, Netherlands); the Huygens tool "PSF distiller" was used to create an experimental PSF from images of 100-nm fluorescent beads that were acquired using the same settings as for the SAM time-lapses. The deconvolved *z*-stacks were corrected for artificial stretching, as described in the pipeline above, then segmented

using the in-house software Constanza (59). The reduction in the signal from the *CLAVATA3* reporter with radial distance from the center of each SAM meant that only the 6-9 cells within a radius of 8 μm of the SAM's center could be accurately segmented (*SI Appendix*, Fig. S23); within this short range, the effect of the diminishing *CLAVATA3* signal on nuclear segmentation accuracy was small (Fig. 3B).

Text S1: Relations between cell volume and surface area growth rates over the cell cycle. Epidermal (L1) SAM cells expand in the plane of the tissue's surface while maintaining an approximately constant height in the perpendicular direction. These geometric constraints, along with the observation that cells do not substantially alter their shape over the cell cycle (Fig. 1A), necessitate the following power-law relations between a cell's volume, V, and the areas of its anticlinal and inner periclinal walls, A_a and A_{ip}, respectively,

$$A_a \sim V^{1/2}, \quad A_{ip} \sim V$$

as validated in *SI Appendix*, Table S7. Similarly, volume was expected to scale proportionally with the outer periclinal wall area A_{op}; data in *SI Appendix*, Table S7 show that the scaling is sub-linear ($A_{op} \sim V^{0.8}$). The total area, A, scales as $A \sim V^{2/3}$, as expected. Given these power-law relations and that volume increases exponentially (at a constant relative rate) over the cell cycle, we have for a given size metric $S \sim V^{\lambda}$

$$d(\ln V)/dt = k \Rightarrow d(\ln S^{1/\lambda})/dt = k \Rightarrow d(\ln S)/dt = k\lambda.$$

Therefore, the wall surface areas A, A_{op}, A_{ip}, and A_a should each increase exponentially over the cell cycle at a relative growth rate that is $\sim$2/3-fold, $\sim$0.8-fold, $\sim$1-fold, and $\sim$1/2-fold the relative growth rate of V respectively. These predictions are corroborated by our data (*SI Appendix*, Fig. S18).

Text S2: Quantitative characterization of cell-size regulation in non-homeostatic conditions. To quantitatively characterize cell-size regulation, it was important to consider cell-size metrics with mean values that do not vary substantially with space across the SAM or with time during data acquisition, since such variability if not properly accounted for can lead to

incorrect conclusions (*SI Appendix*, Fig. S8). First, among L1 cells in the SAM <30 μm from *O* (the center of the SAM which coincides with the peak of *CLAVATA3* expression and slowest cell growth rates), we verified that the normalized cell volume (cell volume divided by mean cell volume at the corresponding time-point *t* denoted μ_V^t) does not vary with space or time (*SI Appendix*, Fig. S3). Second, we reasoned that since sister cells are born simultaneously and at the same position within the SAM, the difference in sister-cell size metrics normalized by the sum of these metrics, $(S - S^{sis})/(S + S^{sis})$ where *S* can correspond to volume *V* or wall areas including *A*, A_a, A_{ip} or A_{op}, should have minimal spatiotemporal variation for all cell-size metrics. *SI Appendix*, Table S2 contains validation of this reasoning; there is a weakly significant variation of $(S - S^{sis})/(S + S^{sis})$ with time that disappears when cells born late in the time-lapse are removed from the sample, indicating that this correlation is an artifact generated by the finite duration of the experiment. Our results are unaffected by whether or not cells born late in the time-lapse are included in the sample (*SI Appendix*, Table S6).

Under the assumption that within a sample all cells grow to the same mean size, a Taylor expansion around the mean birth size characterizes the rule for cell size regulation. Under the assumption of small fluctuations about the mean birth size, a first-order approximation is valid (4),

(1) $S_d \approx \mu^S{}_d + f\,(S_b - \mu^S{}_b) \approx f\,S_b + (\mu^S{}_d - f\,\mu^S{}_b)$,

where S_b, S_d are the cell sizes at birth and division respectively, $\mu^S{}_d$, $\mu^S{}_b$ are the mean division and birth sizes respectively, and *f* is the slope of S_b vs. S_d evaluated at $S_b = \mu^S{}_b$. Substituting Eq. (1) for both a cell and its sister, we obtain a relation between α_d, the sister-size asymmetry at division, and α_b, the sister-size asymmetry at birth,

(2) $\alpha_d = (S_d - S_d^{sis})/(S_d + S_d^{sis}) \approx f \times (S_b + S_b^{sis})/(S_d + S_d^{sis}) \times (S_b - S_b^{sis})/(S_b + S_b^{sis})$

$$= f\,(S_b + S_b^{sis})/(S_d + S_d^{sis})\,\alpha_b.$$

Therefore, under the assumption that α_b^2 is independent of $(S_b + S_b^{sis})/(S_d + S_d^{sis})$ (*SI Appendix*, Fig. S25 shows that, except for A_{ip}, these variables are uncorrelated; the weak correlation for A_{ip} is likely due to outliers; n = 415, p = 0.011-0.99),

$$E[\alpha_d\,\alpha_b] \approx f\ E[(S_b + S_b^{sis})/(S_d + S_d^{sis})\,\alpha_b^2] = f\ E[(S_b + S_b^{sis})/(S_d + S_d^{sis})] \times E[\alpha_b^2],$$

where E[•] denotes the mean. The slope of a least-square linear fit to α_b vs. α_d is given by

$$E[\alpha_d\,\alpha_b]/E[\alpha_b^2] = f\ E[(S_b + S_b^{sis})/(S_d + S_d^{sis})] \approx f/2,$$

due to the observation that for all size metrics, $E[(S_b + S_b^{sis})/(S_d + S_d^{sis})] \approx 1/2$ (*SI Appendix*, Table S5). Similarly, the slope of a least-square linear fit to α_b vs. $\alpha_\Delta = (\Delta - \Delta^{sis})/(\Delta + \Delta^{sis})$, where Δ, Δ^{sis} are the size increments added between birth and division for a cell and its sister, respectively, is given by

$$E[\alpha_\Delta\,\alpha_b]/E[\alpha_b^2] = (1 - f)\ E[(S_b + S_b^{sis})/(\Delta + \Delta^{sis})] \approx 1\text{-}\ f,$$

due to the observation that for all size metrics, $E[(S_b + S_b^{sis})/(\Delta + \Delta^{sis})] \approx 1$ (*SI Appendix*, Table S5).

Data from Tables S3 and S5 show that all cell volume statistics, V_b vs. V_d (normalized and non-normalized) and α_b vs. α_d, consistently predict that $f \approx 0.5$. Surface area size metrics A_{op}, A_{ip}, and A_a change strongly with Euclidean distance from O (Fig. 2A, *SI Appendix*, Fig. S5-S7) so the corresponding f parameters cannot be simply extracted from a plot of e.g. $A_{op,b}$ vs. $A_{op,d}$; for wall area size metrics, f was extracted from plots of α_b vs. α_d and α_b vs. α_Δ by applying the relations above. In all cases, we obtained $f \approx 0.5$ (*SI Appendix*, Table S5). We note that for all size metrics, the division size is the sum of the size of both daughter cells at the time when the new cell wall first becomes visible, i.e. when the new cell wall first becomes detectable by the segmentation

algorithm. Asymmetry statistics included all sister-cell pairs that were tracked over a complete cell cycle within 45 μm of *O*.

Text S3: Simulations of the regulation of cell size and growth. We extended and simulated a stochastic model of cell-autonomous regulation of growth and inter-division timings (4, 37) to compute pairwise correlations among cell-size variables for comparison with our experimental data. In the simulations, each cell from a population of n_{model} cells has a discretized position denoted by x, and is born and divides within a discretized generation denoted by t. For a cell at position x, its dimensionless birth and division sizes are denoted by $S_b(x,t)$ and $S_d(x,t)$, respectively, and the cell grows at a constant relative rate that depends on the degree of asymmetric division of the mother cell for the duration of the cell cycle with an inter-division time of $T(x,t)$. From an initial starting configuration of n_{model} birth sizes at generation $t = 0$, the following equations are iterated for 20 generations, until cell size and inter-division time statistics have reached steady states:

(1) $S_d(x, t) = f\, S_b(x, t) + 2 - f + Z(x, t), \quad Z \sim \mathrm{N}(0, \sigma)$

(2) $T(x, t) = \log_2(S_d/S_b)/(1 - g_{\text{asym}}\, \alpha_b) \quad$ where $\alpha_b(x, t) = (S_b - S_b^{\text{sis}})/(S_b + S_b^{\text{sis}})$

S_b^{sis} being the sister of the cell at (x, t)

for $x = 0, \ldots, n_{\text{model}} - 1$,

(3) for $x < N_{\text{model}}/2, \quad S_b(2x + 1, t + 1) = S_d(x, t)(1/2 + Z_a(x, t))$

$S_b(2x, t + 1) = S_d(x,t)(1/2 - Z_a(x, t)), \quad Z_a \sim \mathrm{N}(0, \sigma_a)$,

i.e., cells at $2x$ and $2x+1$ are sisters.

The fixed parameters f (size regulation), σ (noise), g_{asym} (the strength of the dependence of relative growth rate on mother-cell asymmetric division), and σ_a (frequency of asymmetric

division) are described below. We assumed Gaussian distributions for the noise in cell-size regulation and asymmetric divisions, and a mean cell size and a mean relative growth rate that have no spatiotemporal variation. Pairwise correlations and least-square linear fits between S_b vs. S_d, α_b vs. α_d, and α_b vs. $\alpha_T = (T - T^{sis})/(T + T^{sis})$, where T, T^{sis} are inter-division times of a cell and its sister, respectively, along with other statistics are computed from the final generation of n_{model} cells only. Each instance of the simulation was run with n_{model} cells to approximately match the sample size of the experimental data (n_{model} = 800 for sister asymmetry statistics; n_{model} = 1000 for non-sister asymmetric statistics). Each of the parameters f, σ, σ_a, and g_{asym} were extracted from cell volume experimental data as described below.

Extracting f (the mode of cell size regulation). f is equal to the slope of V_b/μ_V^t vs. V_d/μ_V^t (normalized volumes; *SI Appendix*, Table S3). Bootstrapping (69) the sample of birth and division normalized volumes for L1 central zone cells tracked over a full cell cycle estimated the median (0.48) and 90% confidence interval ([0.42, 0.55]) of f from least- square linear fits to be (0.48, [0.42, 0.55]). Throughout this work, bootstrapping was performed by sampling with replacement from data until the sample size was matched; sampling was repeated 10,000 times to estimate the distribution of the statistic of interest.

Extracting σ (the noise in cell- size regulation). Computing the variance of each side of the equation labeled (1) in the algorithm above gives $\mathrm{var}(S_d) = f^2\,\mathrm{var}(S_b) + \sigma^2$. S_b and S_d are dimensionless size variables corresponding to normalized V_b/μ_b and $V_d/\mu_b \approx V_d/\mu_d \times \mu_d/\mu_b$. Therefore,

$$\sigma^2 \approx (\mu_d/\mu_b)^2\sigma_d^2 - f^2\sigma_b^2,$$

where σ_b and σ_d are the coefficients of variation of cell birth and division normalized volumes, respectively. Bootstrapping the normalized birth and division volumes for L1 central zone cells tracked over a full cell cycle provided estimates of the medians and 90% confidence intervals for σ_d, σ_b, and σ to be (0.14, [0.128, 0.147]), (0.25, [0.239, 0.262]), and (0.227, [0.214, 0.243]), respectively.

Extracting σ_a (the frequency of asymmetric division). The pair of equations labeled (3) in the algorithm above together give

$$\sigma_a^2 = \mathrm{var}((S_b - S_b^{sis})/2(S_b + S_b^{sis})),$$

(*SI Appendix*, Table S1). Bootstrapping the L1 central zone sister-cell pair normalized volumes tracked over a full cell cycle provided estimates of the median and 90% confidence interval of σ_a to be (0.105, [0.099, 0.111]).

Extracting g_{asym} (the strength of the dependence of relative growth rate on mother-cell asymmetric division). Our data indicated that cells grow at a constant relative rate or constant rate per unit size over their cell cycles, with small sisters growing at faster rates than their large sisters. To first order, this dependence can be expressed as

$$g_{\mathrm{rel}}/\mu_g = 1 - g_{\mathrm{asym}}\,\alpha_{b,}$$

where g_{rel} is the relative growth rate and μ_g is the mean growth rate over the entire sample. The mean relative growth rate of normalized volume over the cell cycle was computed as

$$<g_{\mathrm{rel}}>/\mu_g = <(V(t+1)/\mu_V^{t+1} - V(t)/\mu_V^{t})/0.5(V(t+1)/\mu_V^{t+1} + V(t)/\mu_V^{t})>/\mu_g\ .$$

Bootstrapping the sample of (α_b, $<g_{\mathrm{rel}}>/\mu_g$) for L1 central zone sister-cell pairs tracked over a full cell cycle estimated the median and 90% confidence interval of g_{asym}, the negative of the slope of

α_b vs. $\langle g_{rel} \rangle / \mu_g$, from least-square linear fits to be (0.43, [0.365, 0.496]). Note that the deviation in relative growth rates in the relationship between α_b vs. $\langle g_{rel} \rangle / \mu_g$ from $1 - g_{asym}\,\alpha_b$ (inset, Fig. 4A) is partially accounted for by the variation in mean relative growth rate with distance from *O* (*SI Appendix*, Fig. S16). The statistics pertaining to α_b vs. α_T, with which the model is compared, are independent of this spatial variation, and so this effect was not included in the simulations. The medians and 90% confidence intervals of f, σ, σ_a, and g_{asym} derived from bootstrapping were used to generate the plots of Fig. 5 and data in *SI Appendix*, Table S9.

To produce the statistics in *SI Appendix*, Table S9, 1000 simulations generated medians and 90% confidence intervals of various statistics, including the coefficients of variation in cell birth size and cell division size σ_b, σ_d and the least-square linear fit between α_b and α_T. These statistics were in close agreement with the experimental data (Fig. 5, *SI Appendix*, Table S9). In Fig. 5A, trajectories of the ratios of large to small sister-cell sizes over the cell cycle were plotted for a single instance of the simulation using parameter values for the medians of f, σ, σ_a, and g_{asym} estimated from bootstrapping; the inset shows birth size versus division size for a single instance of the simulation. Fig. 5B shows median values and 90% confidence intervals (grey shaded regions) of the statistic specified in each column, as generated by the simulations. In panels (i)-(iii), parameters $\sigma = 0.227$ and $\sigma_a = 0.105$ were held at their experimentally measured values while f (horizontal axes) and g_{asym} (different grey shades; dark to light shades correspond to $g_{asym} = -0.03 - 0.1 \times i$ for $i = 0, \ldots, 8$) were varied. In panels (iv)-(vi), parameters $f = 0.48$ and $\sigma_a = 0.105$ were held at their experimentally measured values while σ (horizontal axes) and g_{asym} (different grey shades; dark to light shades correspond to $g_{asym} = -0.03 - 0.1 \times i$ for $i = 0, \ldots, 8$) were varied. The dashed blue lines (blue shaded regions) denote experimentally measured

medians (90% confidence intervals) for parameters estimated by bootstrapping, and the dashed red lines (red shaded regions) denote experimentally measured medians (90% confidence intervals) for the statistic specified in each column.

Our simulations indicate that the experimental data is consistent with a cell-autonomous model of the regulation of growth and size, and that the dependence of relative growth rate on the mother-cell asymmetric division, parametrized by g_{asym}, is required to account for the statistical trends in the experimental data.

References:

61. Thevenaz P, Ruttimann UE, & Unser M (1998) A pyramid approach to subpixel registration based on intensity. *IEEE Trans. Image Process.* 7(1):27-41.

62. Ourselin S, Roche A, Prima S, & Ayache N (2000) Block matching: A general framework to improve robustness of rigid registration of medical images. in *International Conference on Medical Image Computing and Computer-Assisted Intervention.* (Springer Berlin Heidelberg), pp 557-566.

63. Commowick O, Grégoire V, & Malandain G (2008) Atlas-based delineation of lymph node levels in head and neck computed tomography images. *Radiother. Oncol.* 87(2):281-289.

64. Michelin G*, et al.* (2016) Spatiotemporal registration of 3D microscopy image sequences of Arabidopsis floral meristems. In *IEEE 13th International Symposium on Biomedical Imaging (ISBI)* pp. 1127-1130.

65. Thompson KE (2007) Computing particle surface areas and contact areas from three-dimensional tomography data of particulate materials. *Part. Part. Syst. Charact.* 24(6):440-452.

66. Lindblad J (2005) Surface area estimation of digitized 3D objects using weighted local configurations. *Image Vis. Comput.* 23(6):111-122.

67. Windreich G, Kiryati N, & Lohmann G (2003) Voxel-based surface area estimation: from theory to practice. *Pattern Recogn.* 36(11):2531-2541.

68. Schroeder W, Martin K, & Lorensen B (2006) *The Visualization Toolkit* (Kitware, Inc., New York) 4th Ed.

69. Efron B (1979) Bootstrap methods: Another look at the jackknife. *Ann. Stat.* 7(1):1-26.

Supplementary Figures:

In all supplementary figures and tables, *N* is the sample size; sl., int. are the slope and intercept, respectively, of a least-square linear fit; *R* is the Pearson correlation coefficient with a corresponding *p*-value denoted by *p*.

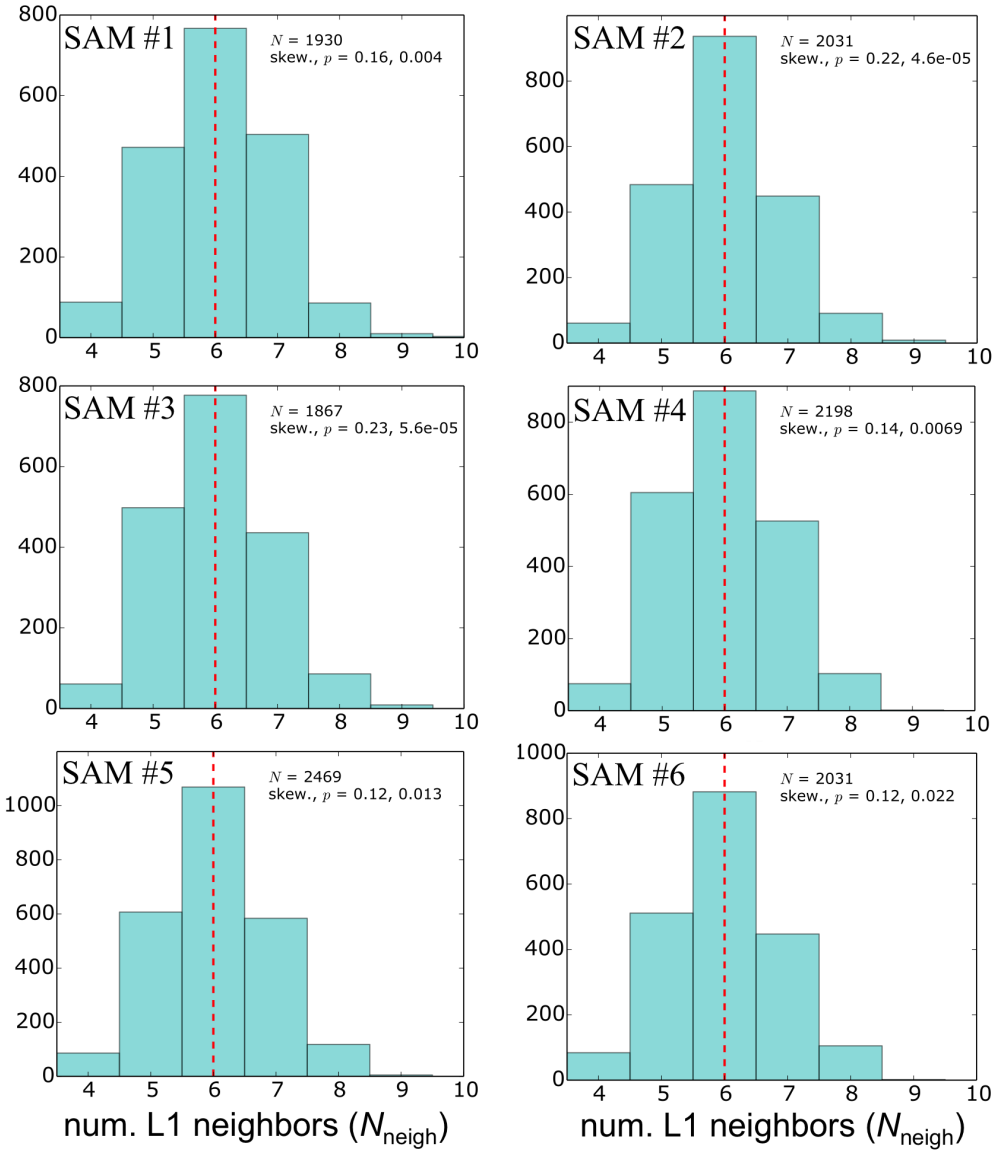

Fig. S1: Number of neighbor distributions in the meristem epidermis. The time-averaged distributions of number of L1 neighbors (N_{neigh}) for cells in the central zone are similar to those of other studies (32, 33), with medians (red dashed lines) of six L1 neighbors for all SAMs. Number of L1 neighbors for cells <30 μm from *O* and for all time-points were amalgamated to generate these histograms.

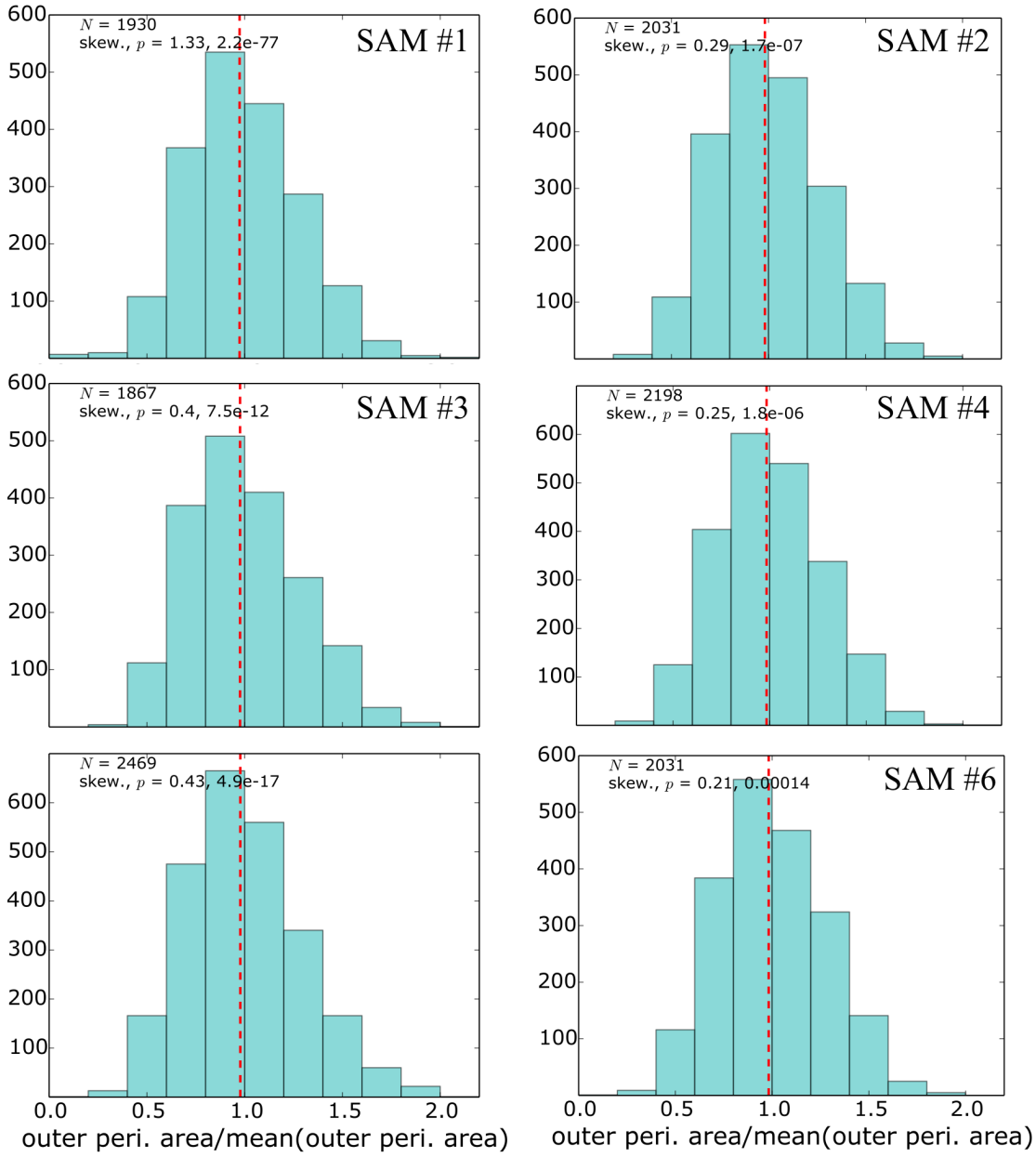

Fig. S2: Periclinal wall area distributions. The time-averaged distributions of outer periclinal wall areas of L1 central zone cells that are similar to other studies (34), with weighted left tails as demonstrated by the significant positive skewnesses,. All cells <30 μm from *O* and all time-points were amalgamated to generate these histograms.

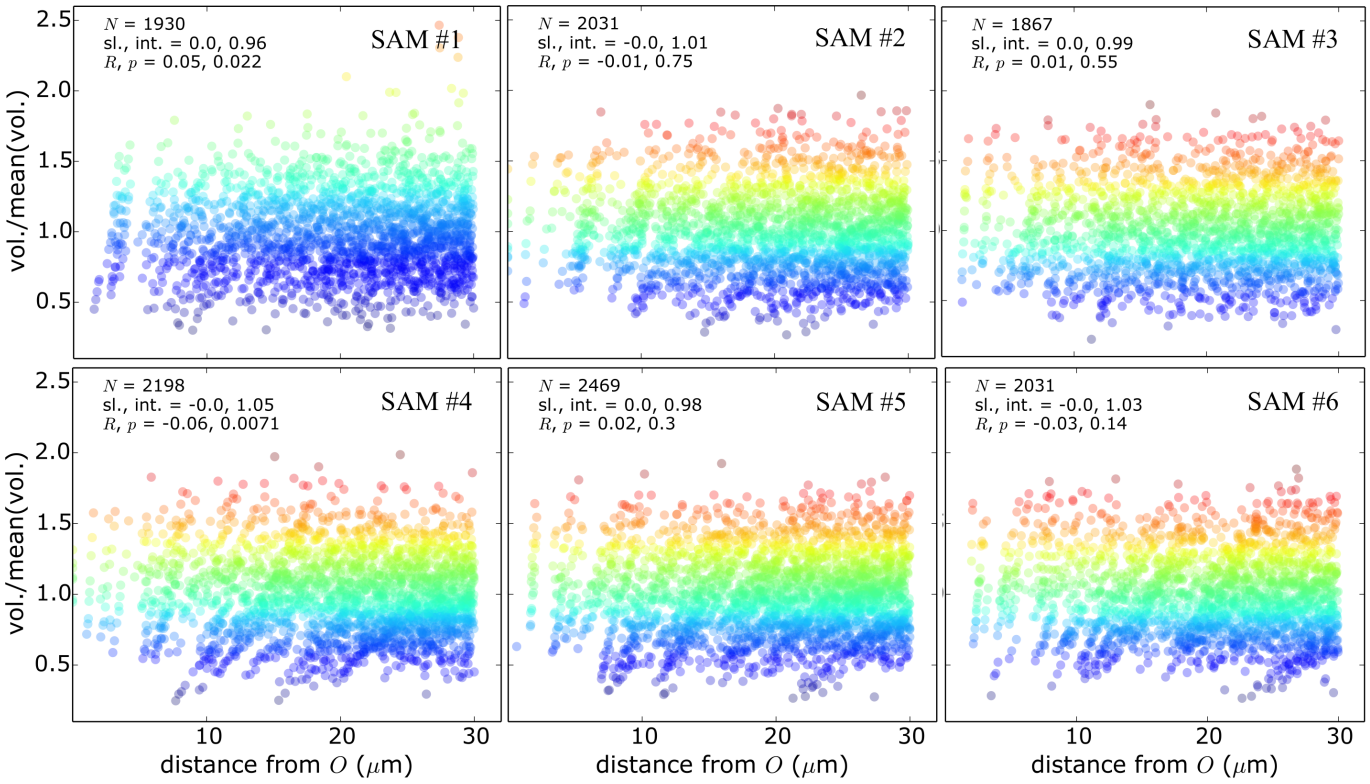

Fig. S3: Mean cell volume did not vary with position in SAM central zones. For each SAM central zone (cells within radius 30 μm of the SAM center at *O*), cell volumes (*V*) are constant with Euclidean distance from *O*. Data from each time-point were amalgamated to generate these plots. Cells are colored according to cell volume, with each panel corresponding to a distinct SAM.

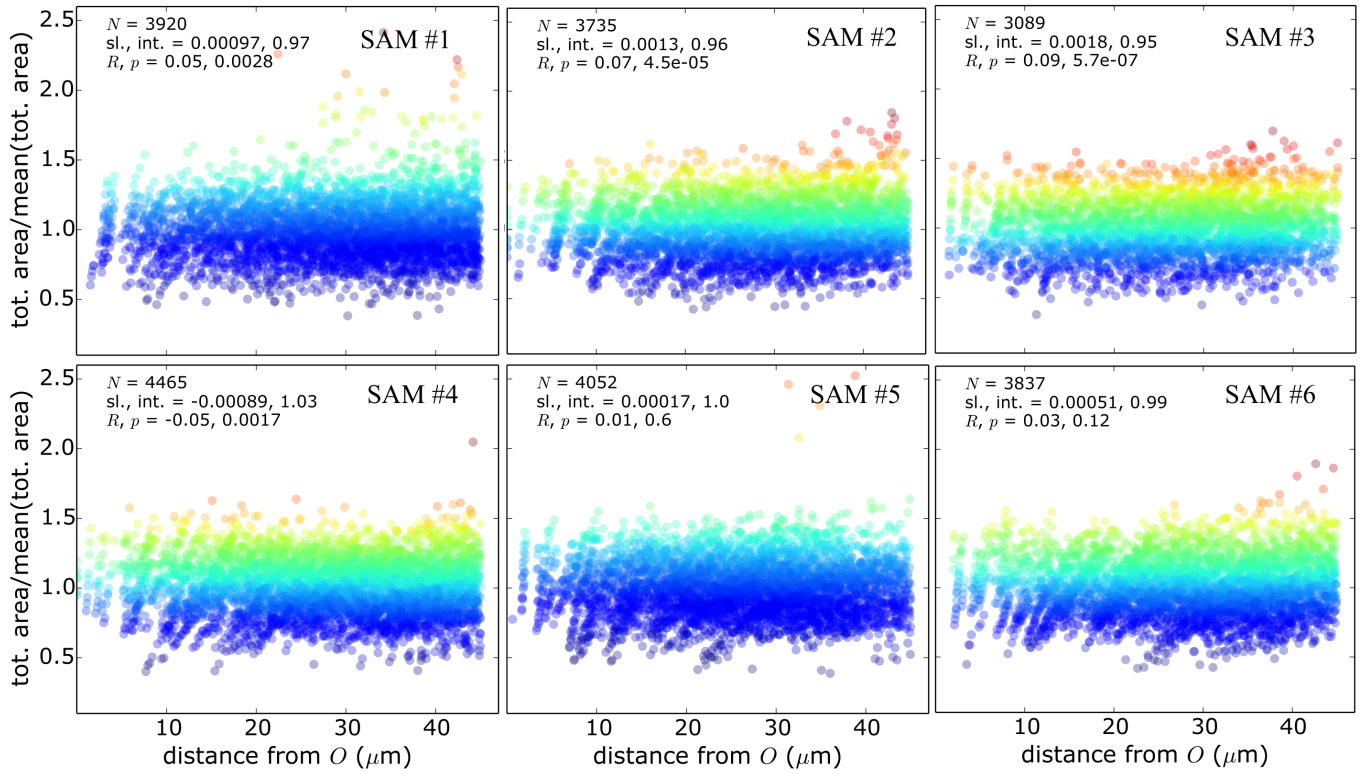

Fig. S4: Mean total cell wall area did not vary with position in SAM central zones. For each SAM central zone, total surface areas (*A*) are constant with Euclidean distance from *O*. Data from each time-point were amalgamated to generate these plots. Cells are colored according to volume (as in Fig. S3), with each panel corresponding to a distinct SAM.

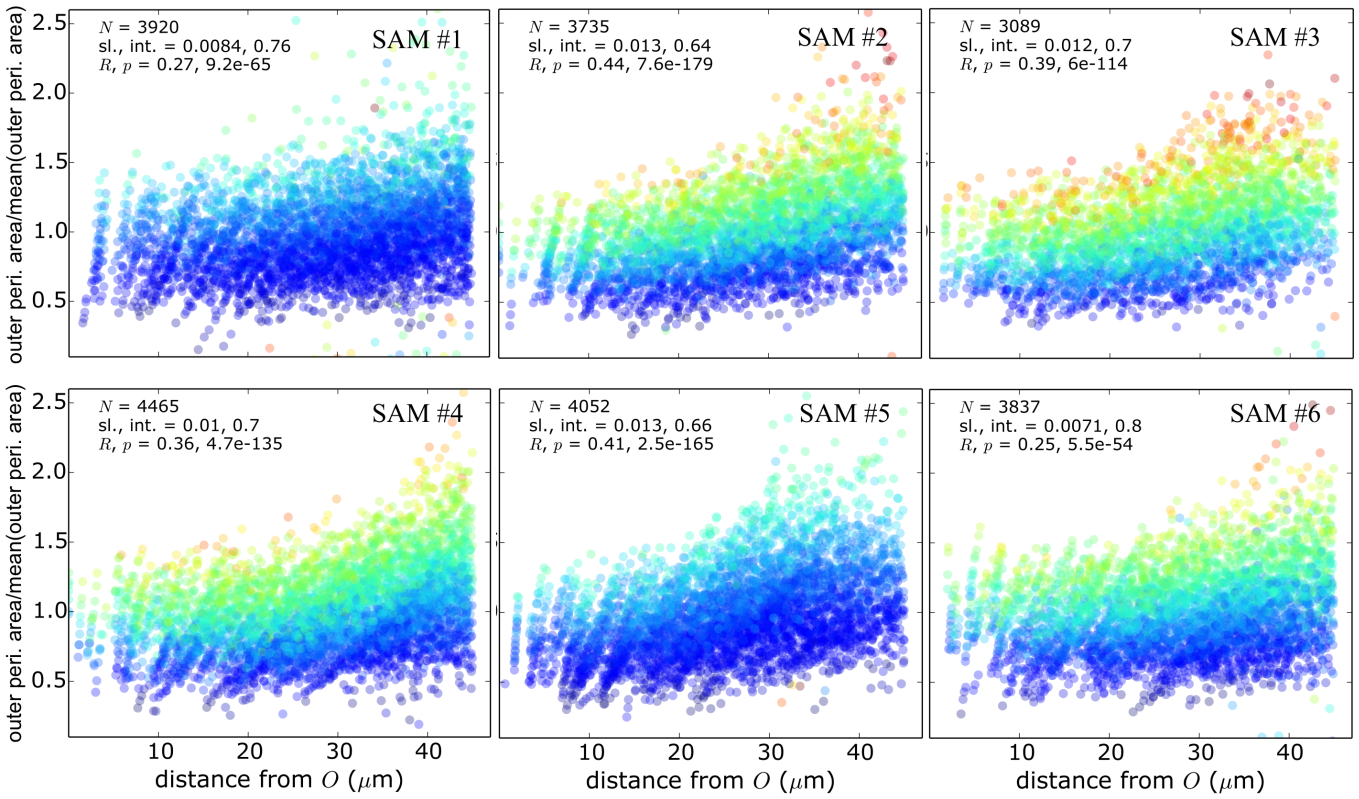

Fig. S5: Mean outer periclinal wall area increased with distance from the SAM center. For each SAM central zone, outer periclinal wall areas (A_{op}) increase with distance from *O*. The slope from a least-square linear fit indicated that outer periclinal wall areas change by ~1.6-fold between the center and the periphery of the SAM, with most of the change occurring between 30 and 45 μm. Data from each time-point were amalgamated to generate these plots. Cells are colored according to volume (as in Fig. S3), with each panel corresponding to a distinct SAM.

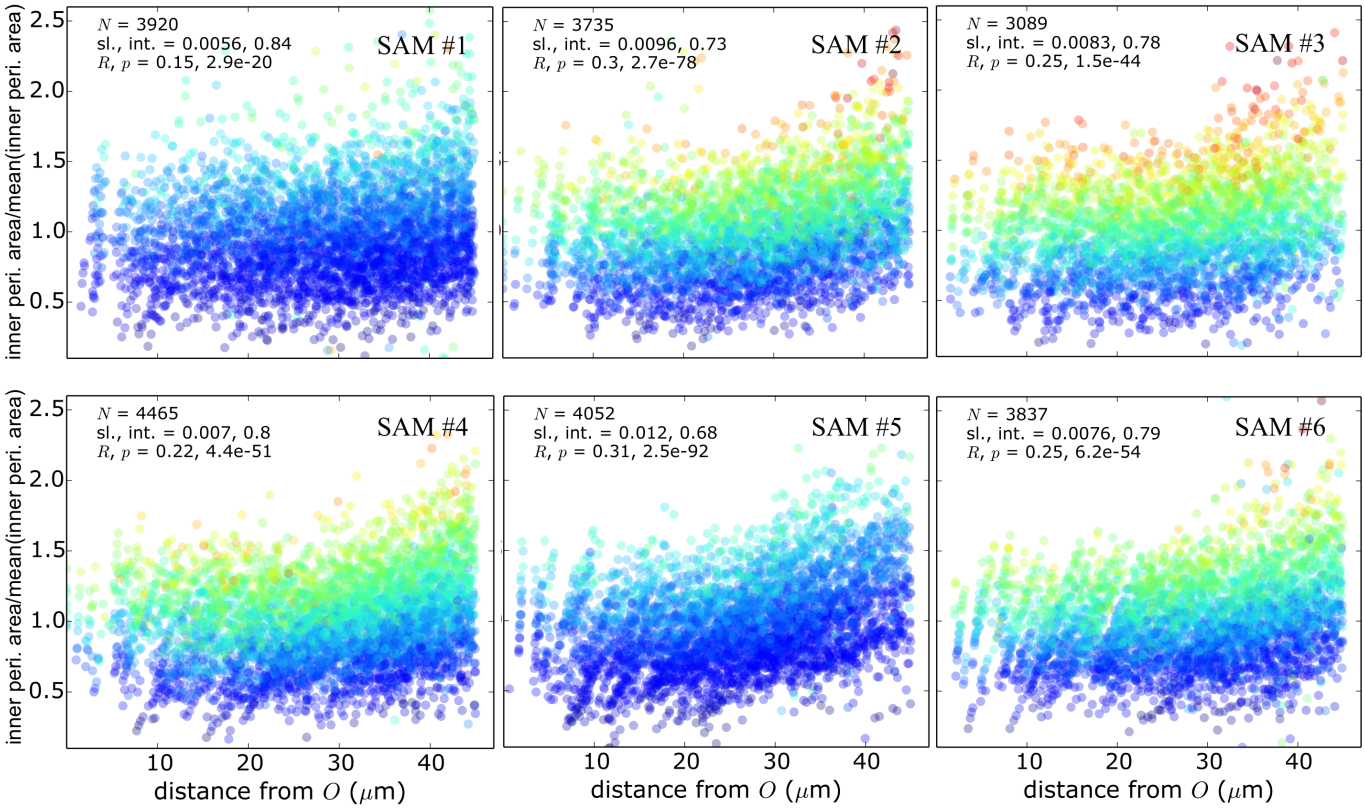

Fig. S6: Mean inner periclinal wall area increased with distance from the SAM center. For each SAM central zone, inner periclinal wall areas (A_{ip}) change by ~1.6-fold between the center and the periphery of the SAM, with most of the change occurring between 30 and 45 μm. Data from each time-point were amalgamated to generate these plots. Cells are colored according to volume (as in Fig. S3), with each panel corresponding to a distinct SAM.

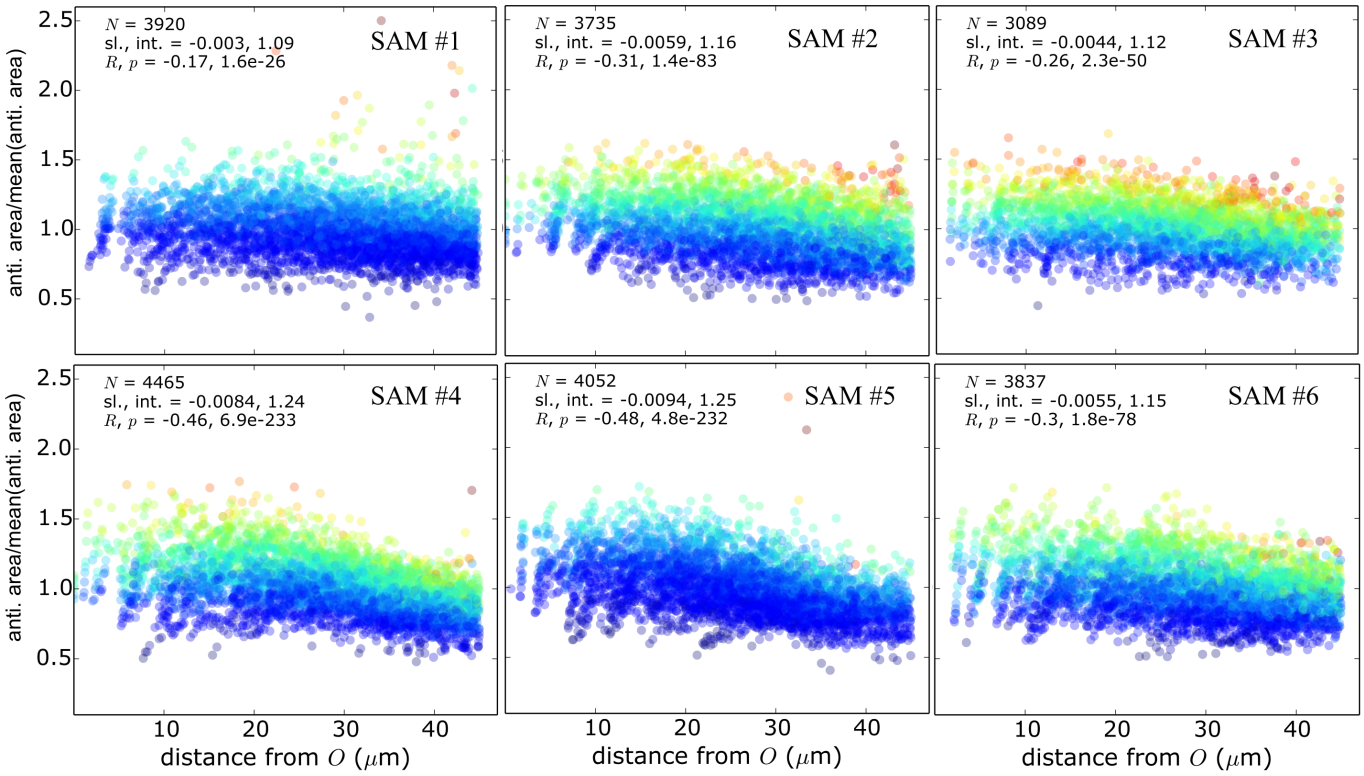

Fig. S7: Mean anticlinal wall area decreased with distance from the SAM center. For each SAM central zone, anticlinal wall areas (A_a) change by ~0.8-fold, with most of the change occurring between 30 and 45 μm. Data from each time-point were amalgamated to generate these plots. Cells are colored according to volume (as in Fig. S3), with each panel corresponding to a distinct SAM.

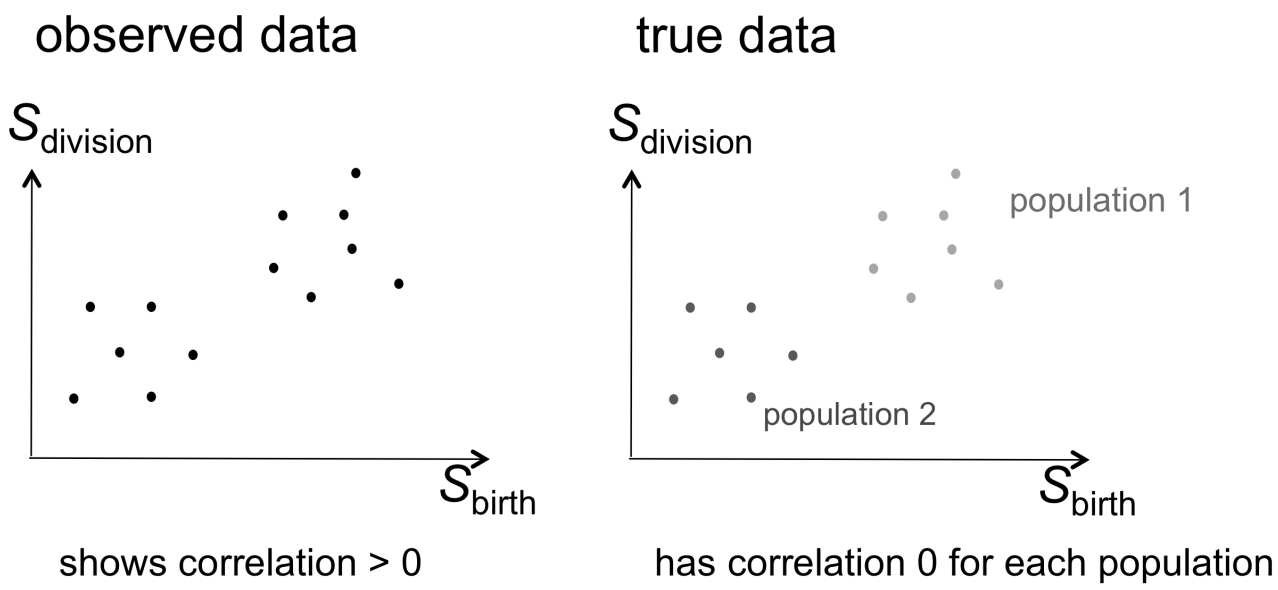

Fig. S8: Previous studies relied on cell size homeostasis to infer the rule for size regulation. In studies of single-celled organisms in homeostatic environments, to determine whether cells regulate their size according to a critical size, critical increment, or fixed time mode, birth size is compared against division size/size increment: a positive/zero correlation implies a critical increment mode, while a zero/negative correlation implies a critical size mode. However, if the data set is comprised of two or more populations with some cells growing to a larger mean target size, the presence of multiple populations may generate correlations among birth and division size metrics, potentially leading to incorrect conclusions about the mode of size regulation. Therefore, since in our data some cell size metrics have spatiotemporal variation, it was important to focus on cell size statistics chosen to eliminate this variation.

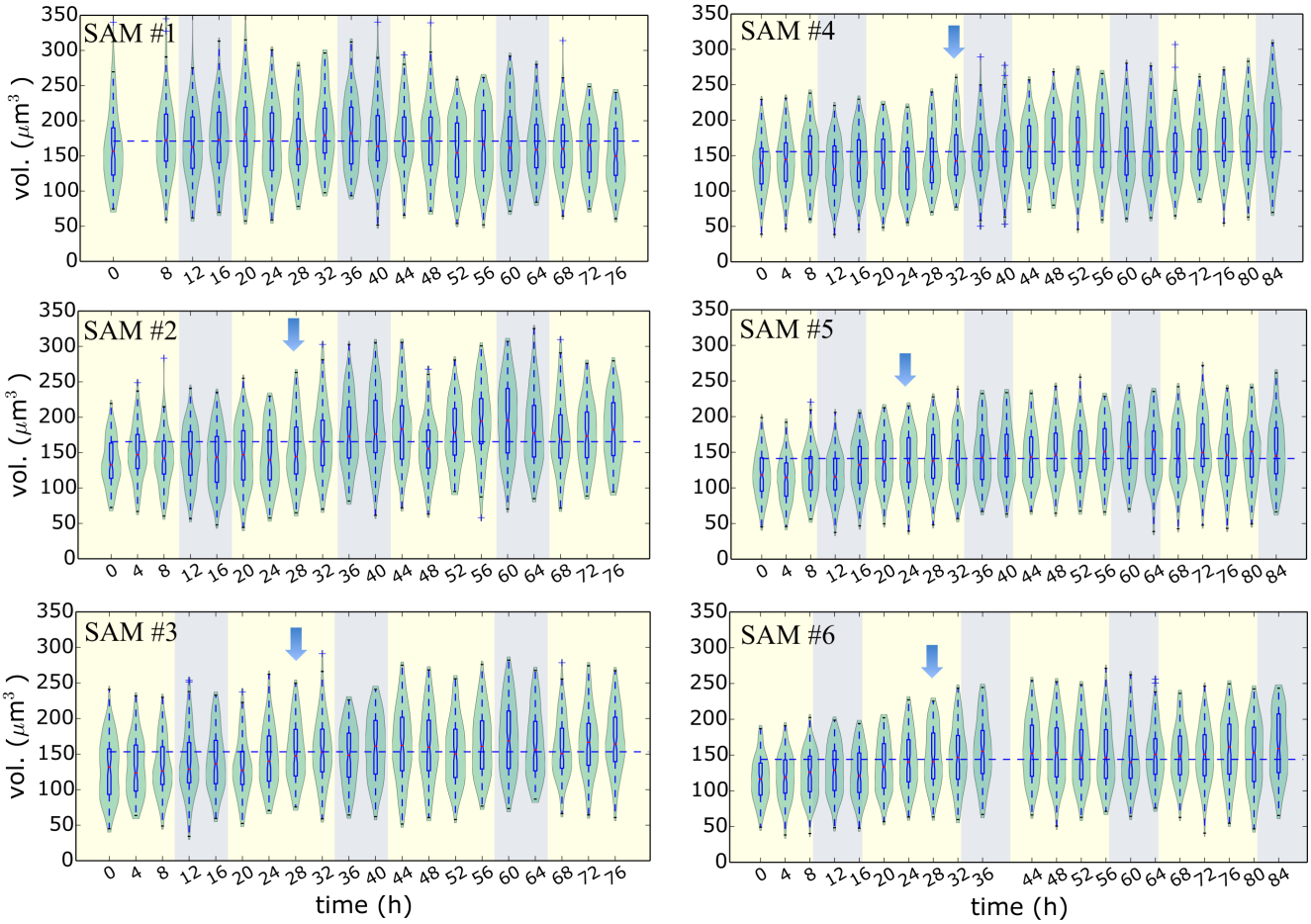

Fig. S9: Cell volume varied over time in individual SAMs. In 5/6 SAMs, a ~20% increase in mean volume of L1 cells in the central zone (blue arrows) occurred 16-32 h into the time-lapse. The horizontal blue dashed line indicates the mean volume of the time-averaged distribution of central zone L1 cell volumes. Yellow/blue shading corresponds to 16 h/8 h periods of light/dark.

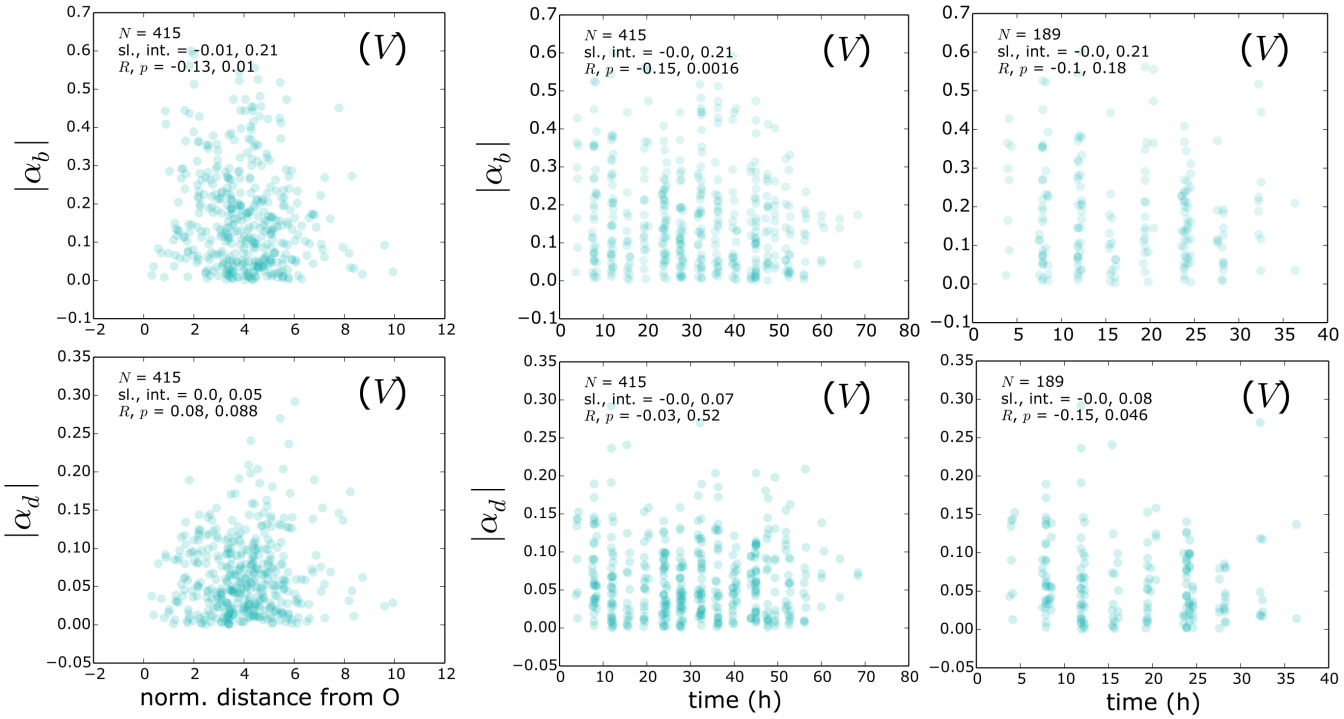

Fig. S10: Sister-volume asymmetry statistics have minimal spatiotemporal variation that does not affect results. There is no correlation between Euclidean distance from *O*, measured for each SAM in units of (median cell volume)$^{1/3}$, and sister-volume asymmetry ($|(V-V^{sis})/(V+V^{sis})|$). This conclusion is valid at both birth (top row, $|\alpha_b|$) and division (bottom row, $|\alpha_d|$), see also Table S2. There is a weak correlation with time at birth. However, this correlation is an artifact due to the finite duration of the experiment, and it disappeared when cells born late in the time-lapse were removed from the data set (removing cells born after t_{med}~35 h leaves ~50% of data points; right column), while the correlations among these statistics, from which the mode of cell size regulation were inferred, were unaffected (Table S6). The plots show data from all pairs of sisters that completed cell cycles that began <45 μm from *O*.

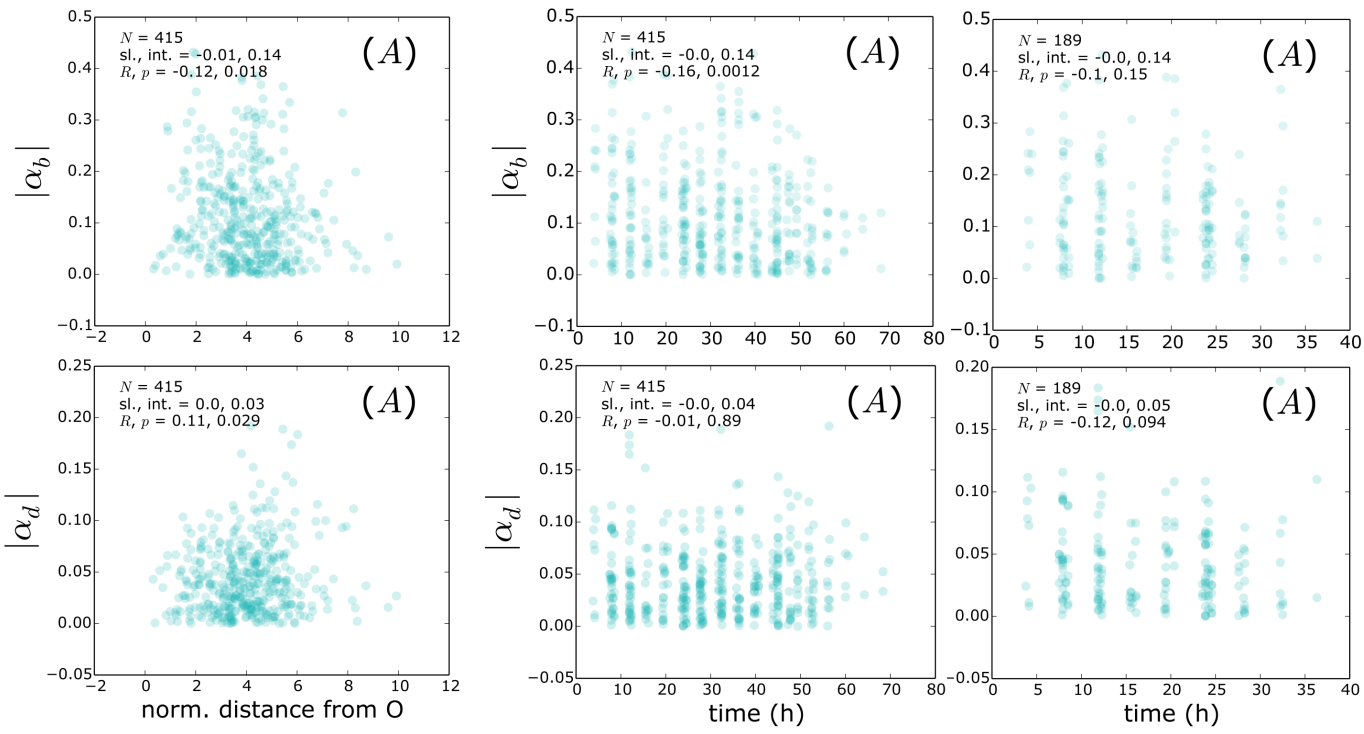

Fig. S11: Sister-wall surface area asymmetry statistics have minimal spatiotemporal variation that does not affect results. There is no correlation between Euclidean distance from *O*, measured for each SAM in units of (median cell volume)$^{1/3}$, and the sister-total wall area asymmetry ($|(A-A^{sis})/(A+A^{sis})|$) at both birth (top row, $|\alpha_b|$) and division (bottom row, $|\alpha_d|$), see also Table S2. As in Fig. S10, the weak correlation with time at birth is an artifact due to the finite duration of the experiment; it disappeared when cells born late in the time-lapse were removed from the data set (right column), while the correlations among these statistics, from which the mode of cell size regulation were inferred, were unaffected (Table S6). The plots show data from all pairs of sisters that completed cell cycles that began <45 μm from *O*.

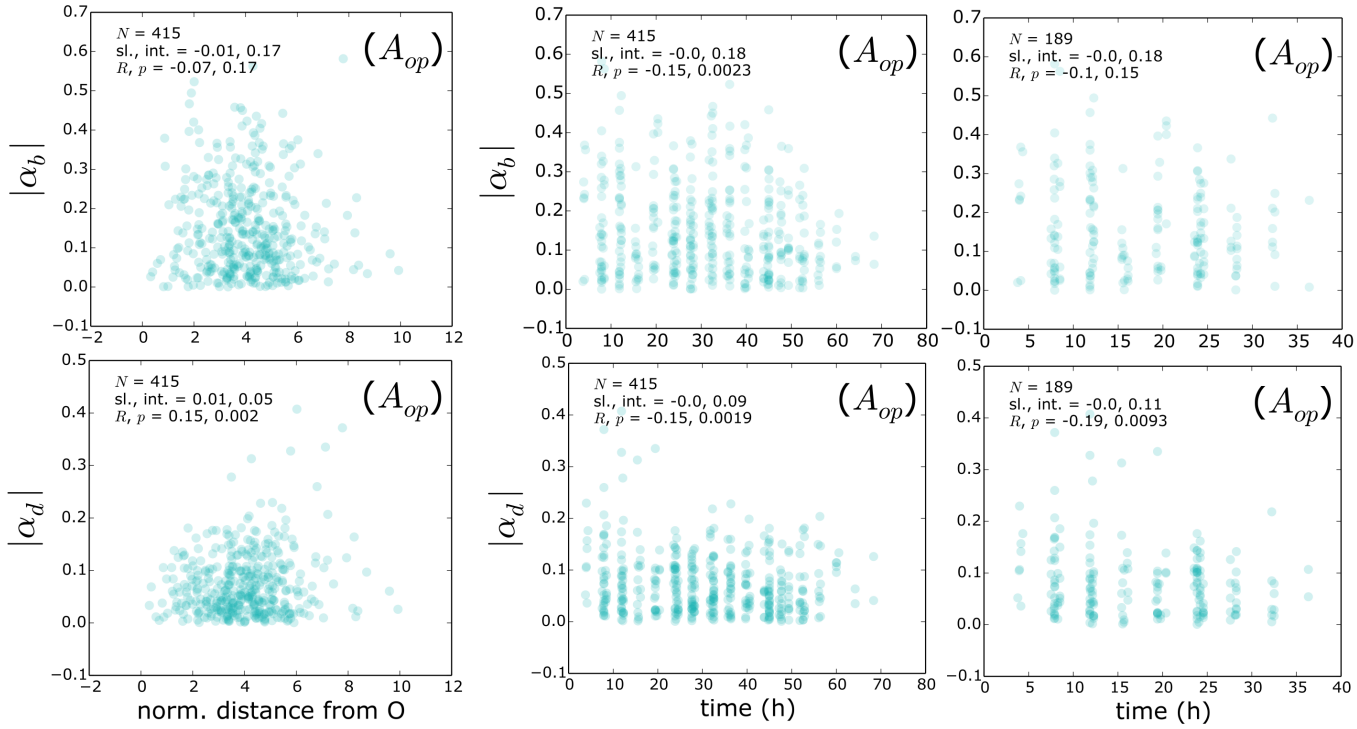

Fig. S12: Sister-outer periclinal wall area asymmetry statistics have minimal spatiotemporal variation that does not affect results. There is a weak correlation between Euclidean distance from *O*, measured for each SAM in units of (median cell volume)$^{1/3}$, and the sister-outer periclinal wall area asymmetry statistics ($|(A_{op}-A_{op}^{sis})/(A_{op}+A_{op}^{sis})|$). There is no correlation at birth (top row, $|\alpha_b|$), and a weak correlation at division owing to a small number of data points (bottom row, $|\alpha_d|$), see also Table S2. As in Fig. S10, the weak correlation with time at birth is an artifact due to the finite duration of the experiment; it disappeared when cells born late in the time-lapse were removed from the data set (right column), while the correlations among these statistics, from which the mode of cell size regulation were inferred, were unaffected (Table S6). The plots show data from all pairs of sisters that completed cell cycles that began <45 μm from *O*.

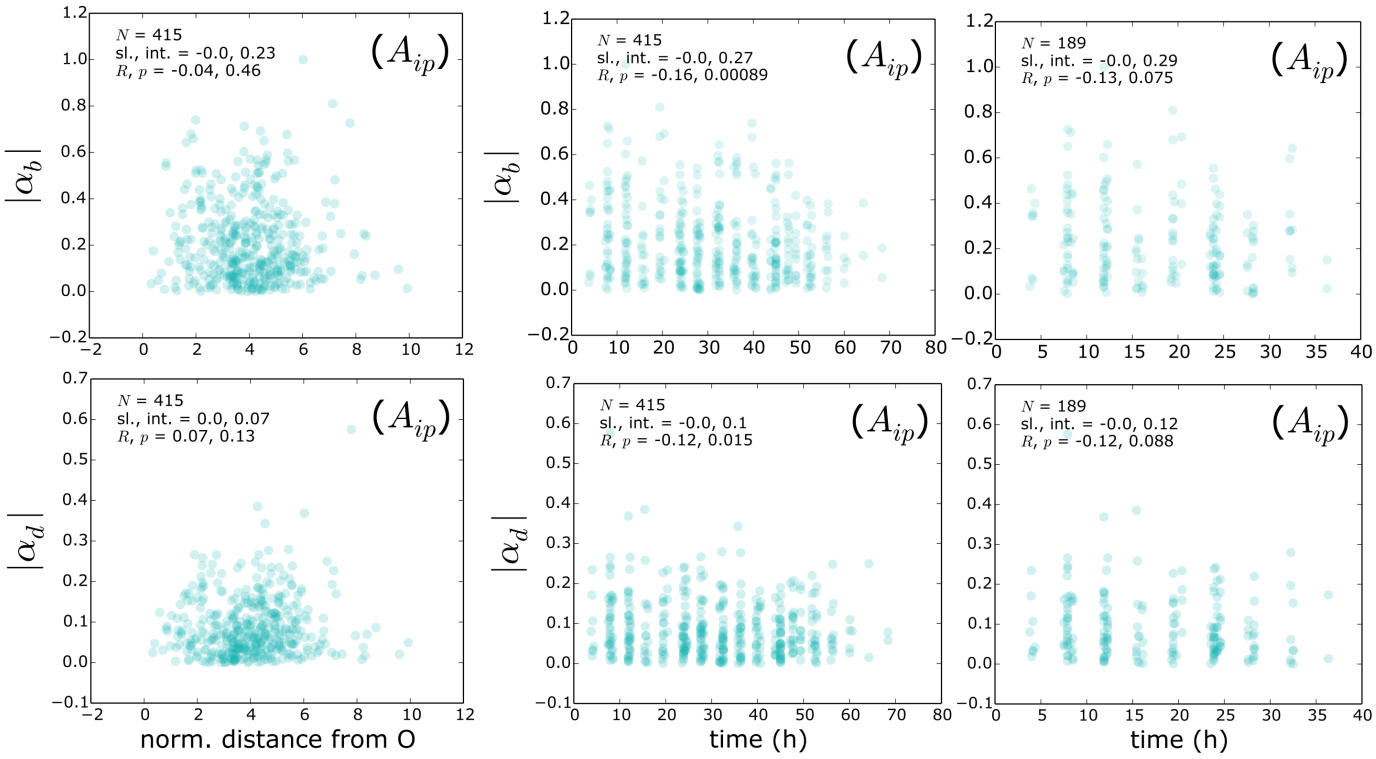

Fig. S13: Sister-inner periclinal wall area asymmetry statistics have minimal spatiotemporal variation that does not affect results. There is no correlation between Euclidean distance from *O*, measured for each SAM in units of (median cell volume)$^{1/3}$, and the sister-inner periclinal wall area asymmetry statistics ($|(A_{ip}-A_{ip}^{sis})/(A_{ip}+A_{ip}^{sis})|$) at both birth (top row, $|\alpha_b|$) and division (bottom row, $|\alpha_d|$), see also Table S2. As in Fig. S10, the weak correlation with time at birth is an artifact due to the finite duration of the experiment; it disappeared when cells born late in the time-lapse were removed from the data set (right column), while the correlations among these statistics, from which the mode of cell size regulation were inferred, were unaffected (Table S6). The plots show data from all pairs of sisters that completed cell cycles that began <45 μm from *O*.

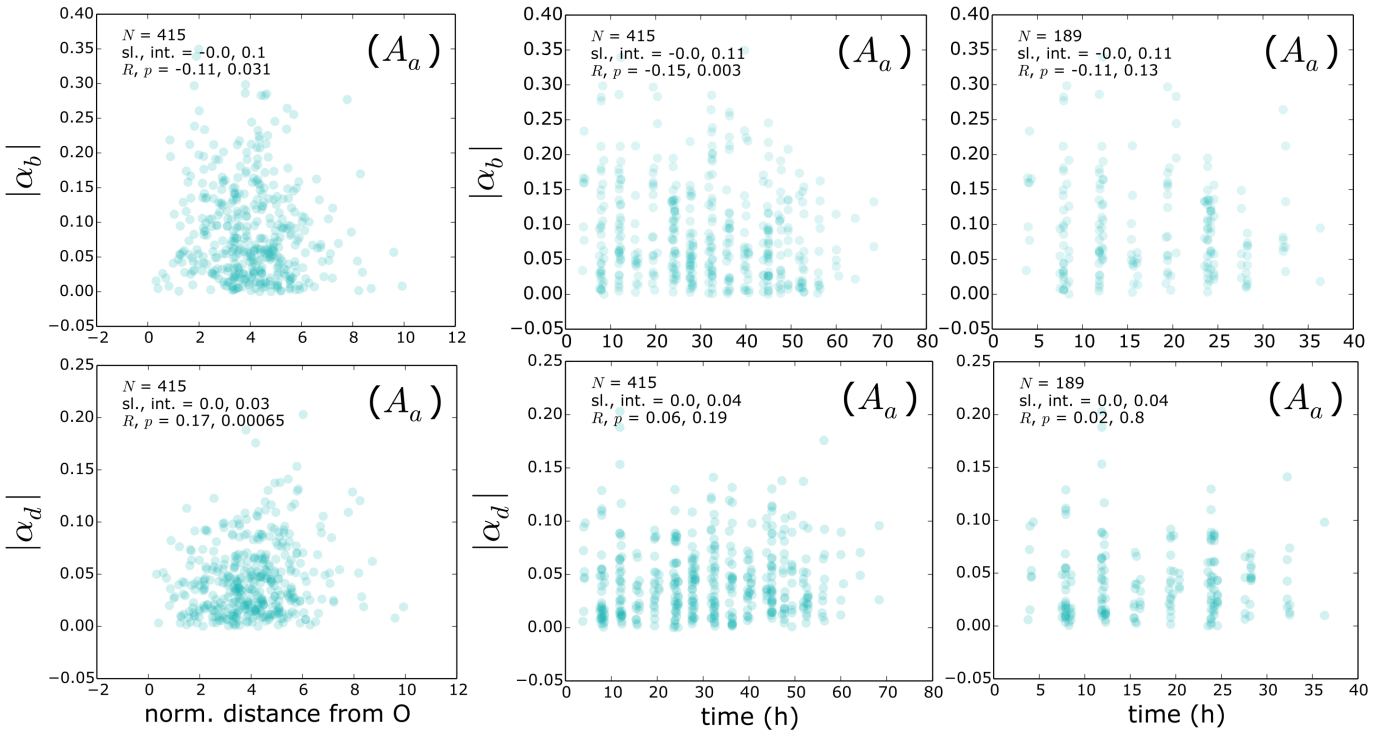

Fig. S14: Sister-anticlinal wall area asymmetry statistics have minimal spatiotemporal variation that does not affect results. There is no correlation between Euclidean distance from *O*, measured for each SAM in units of (median cell volume)$^{1/3}$, and the sister-anticlinal wall area asymmetry statistics ($|(A_a\text{-}A_a^{sis})/(A_a+A_a^{sis})|$) at both birth (top row, $|\alpha_b|$) and division (bottom row, $|\alpha_d|$), see also Table 2. As in Fig. S10, the weak correlation with time at birth is an artifact due to the finite duration of the experiment; it disappeared when cells born late in the time-lapse were removed from the data set (right column), while the correlations among these statistics, from which the mode of cell size regulation were inferred, were unaffected (Table S6). The plots show data from all pairs of sisters that completed cell cycles that began <45 μm from *O*.

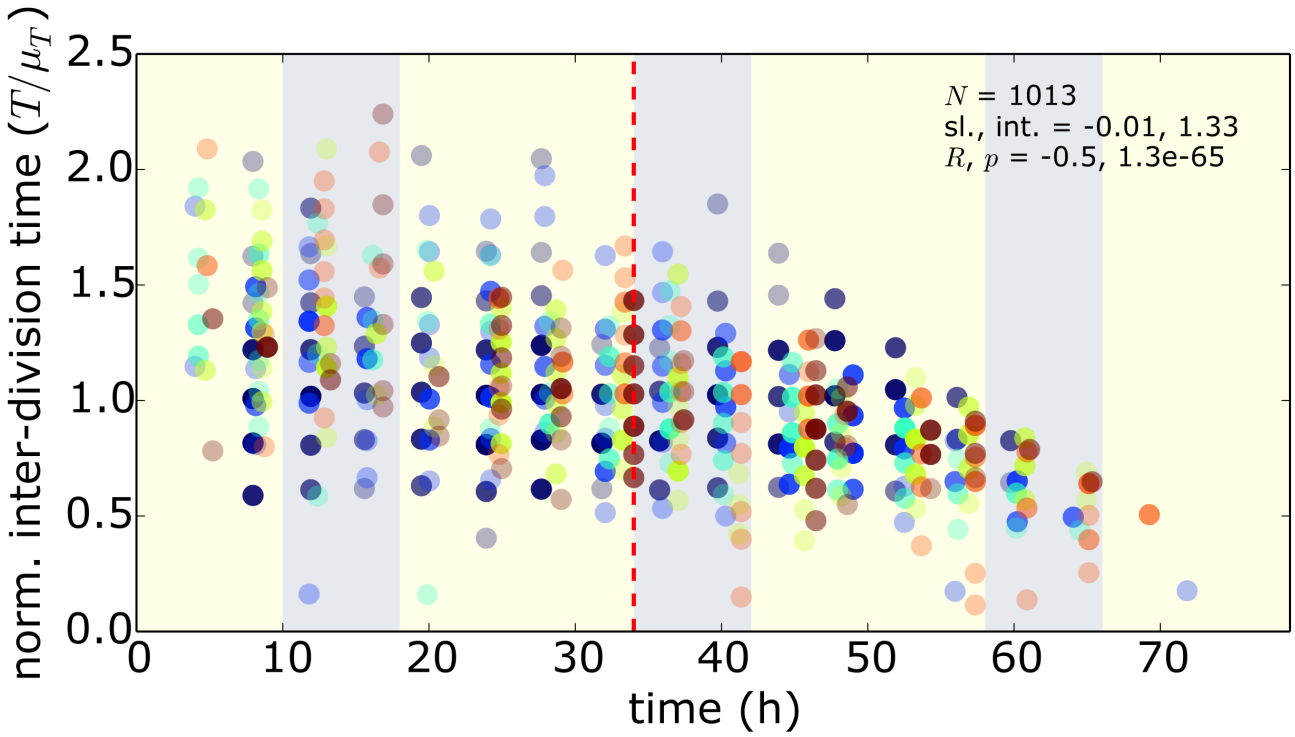

Fig. S15: The mean inter-division time of L1 central zone cells decreases over the time-lapse from ~35 h onward (red dashed line). This decrease occurred because within ~1 cell cycle of the end of the time-lapse, cells with rapid cell cycles are more likely to be sampled. This bias did not affect any of our conclusions (Table S6). Data points are colored according to SAMs.

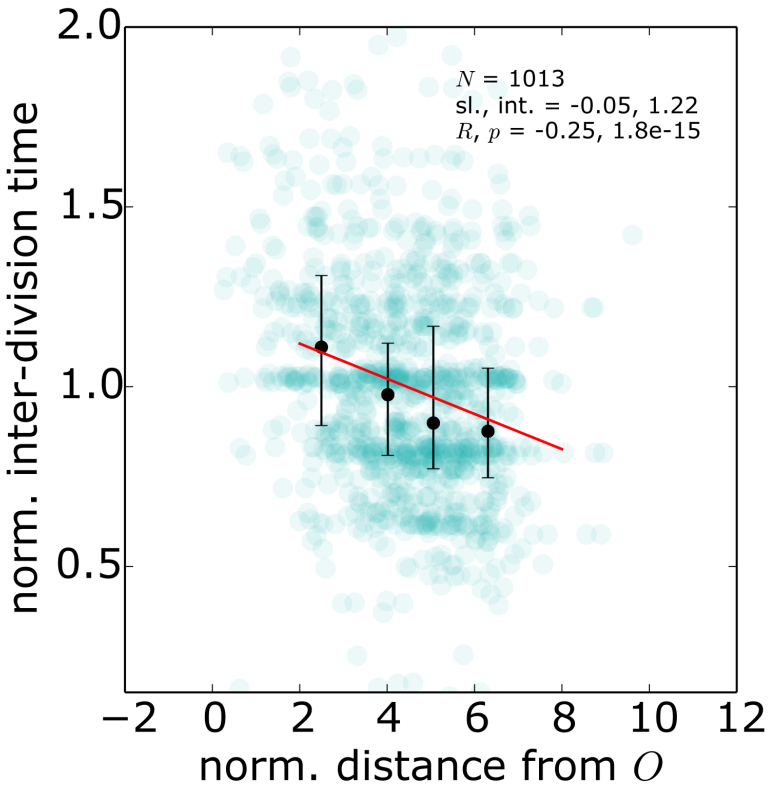

Fig. S16: Quantitative relation between cell growth rate and distance from the SAM center. The inter-division times among L1 central zone cells decrease with distance from the center of the SAM at *O*, normalized by (median cell volume)$^{1/3,}$ at a rate of ~5% between neighboring cells. The red line is the least-square linear fit and the error bars show medians of inter-division times when binned according to normalized distance.

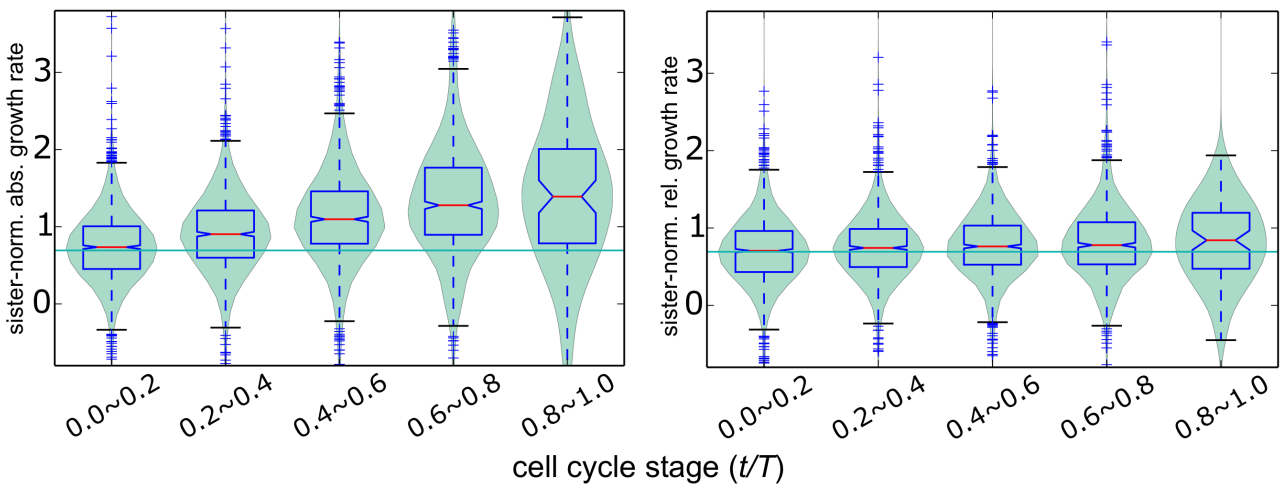

Fig. S17: Cell volume grows proportionally to volume. The volumetric absolute growth rate normalized by the average inter-division time of a cell and its sister (T^{sis}) increases by ~2-fold over the cell cycle (absolute growth rate = $dV/dt \times T^{sis}/\mu_b$), while the volumetric relative growth rate normalized by the average inter-division time of a cell and its sister (T^{sis}) remains constant (relative growth rate = $dV/dt \times T^{sis}/V$) throughout the cell cycle (as a function of t/T, where $t = 0$ is the time of cell birth and T is the inter-division time) at the expected value of ln(2) (green horizontal line) for normalized volume $V/\mu_V{}^t$. The purpose of normalizing by T^{sis} was to partially eliminate the effect of the spatiotemporal variation in growth rates on these statistics: the statistic provides a local measure of cell doubling time, since sister cells, which are often generated by asymmetric divisions, are born in the same position and at the same time. In sum, the plots demonstrate that cell volume grows proportionally to volume.

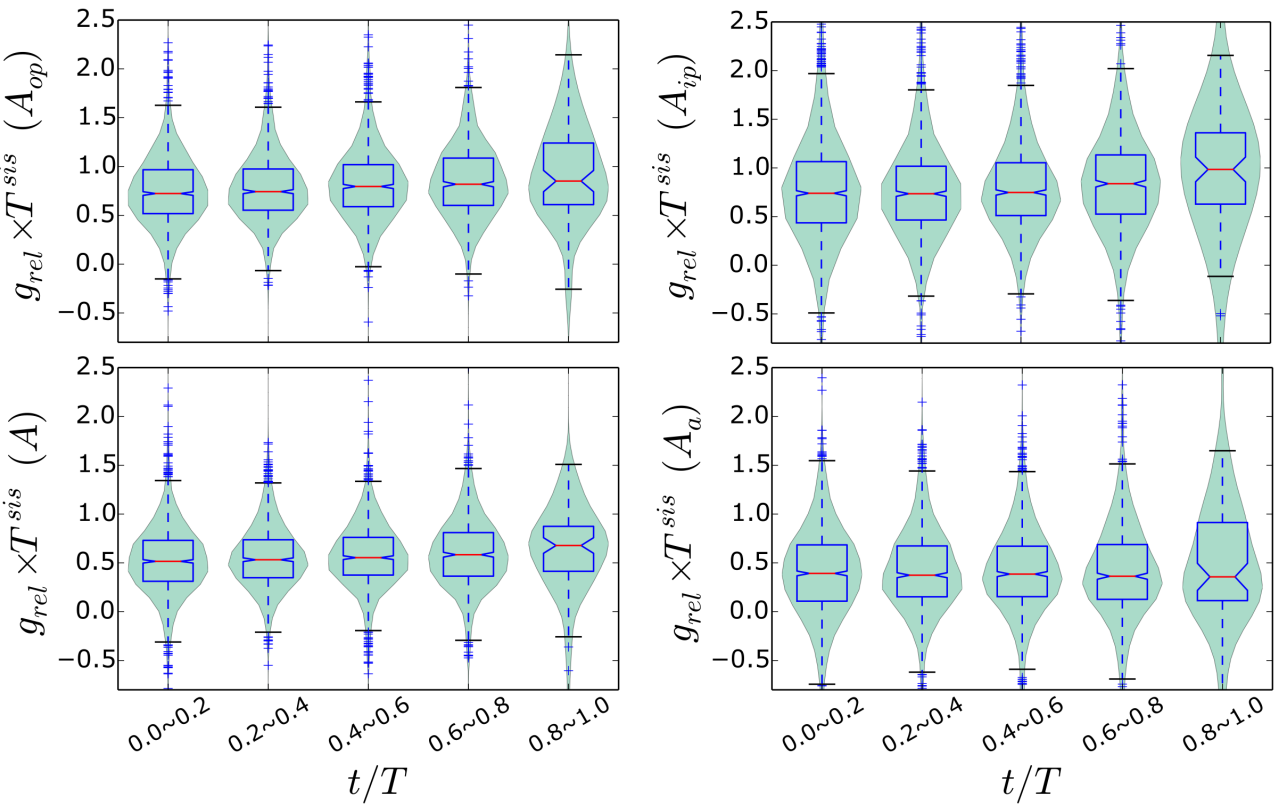

Fig. S18: Cell size grows at a constant relative rate for different wall area cell size metrics. The constant relative volumetric growth rate over the cell cycle and the power-law relationships between cell volume and wall surface area measurements (total surface area $A \sim V^{2/3}$, outer periclinal wall surface area $A_{op} \sim V^{0.8}$, inner periclinal wall surface $A_{ip} \sim V$, and anticlinal wall area $A_a \sim V^{0.5}$) predict that each measure of wall surface area S also grows at a constant relative rate over the cell cycle: $g_{rel} = dS/dt \times 1/S$ = constant. The plots show that the sister-normalized relative growth rates $g_{rel} \times T^{sis}$ (where T^{sis}, the average inter-division time of the cell and its sister, partially factors out the increase in growth rates with radial distance from the SAM's center at O) are approximately constant over the cell cycle (as a function of t/T, where $t = 0$ is the time of cell birth and T is the inter-division time) for each wall surface area measurement as predicted.

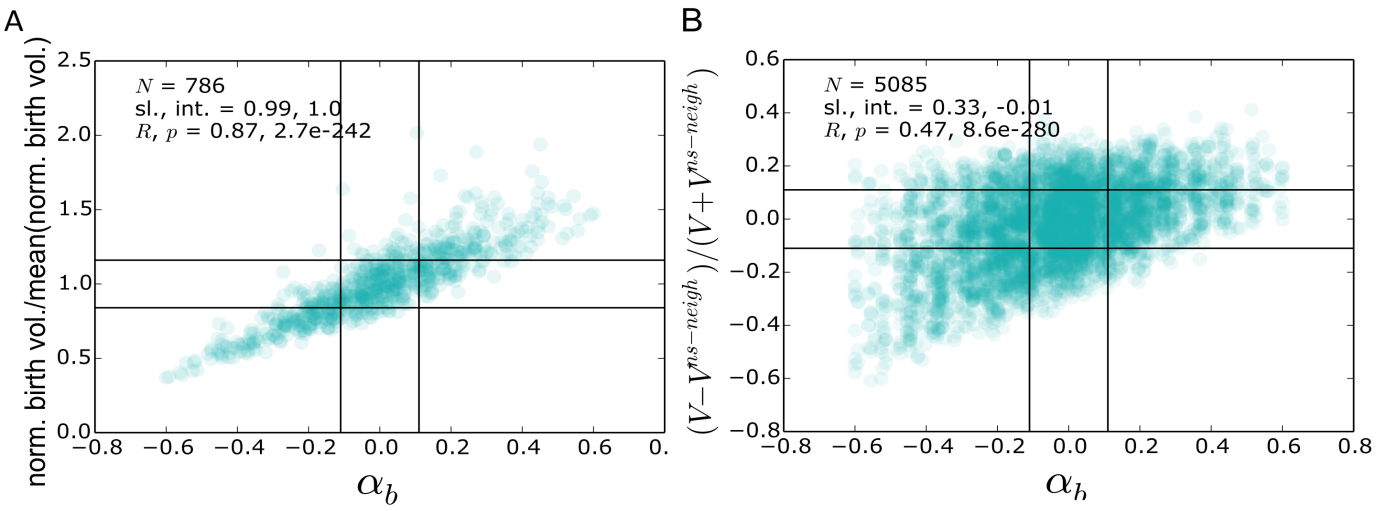

Fig. S19: Asymmetric division is correlated with cell-size and the size of a cell compared with its non-sister neighbors. There is a strong correlation between the degree of asymmetric division, measured by $\alpha_b = (V_b - V_b^{sis})/(V_b + V_b^{sis})$, and (A) normalized birth volume $(V_b/\mu_V^t)/\text{mean}(V_b/\mu_V^t)$ (R = 0.87, $p = 10^{-242}$), and (B) the relative volume of a cell compared with its *non-sister* neighbors, quantified by $(V - V^{ns\text{-}neigh})/(V + V^{ns\text{-}neigh})$, where V is the cell's volume and $V^{ns\text{-}neigh}$ is the average volume of its non-sister neighbors (R = 0.47, $p = 10^{-280}$). The plots show data from all pairs of sisters that completed cell cycles that began <30 μm from *O*. Vertical lines correspond to α_b = -0.11 and α_b = 0.11; cells that have $|\alpha_b| \leq 0.11$ or $|\alpha_b| > 0.11$ were considered to have been born from a symmetric or asymmetric division of the mother cell, respectively; using this definition, the data were split ~50:50 according to whether cells were born of a symmetric or asymmetric division. Similarly, the horizontal lines in (A) split the data ~50:50 according to whether cells were born with intermediate volumes, $|V_b/\mu_V^t/\text{mean}(V_b/\mu_V^t) - 1| \leq 0.16$, or small/large volumes, $|V_b/\mu_V^t/\text{mean}(V_b/\mu_V^t) - 1| > 0.16$; the horizontal lines in (B) split the data ~50:50 according to whether cells of volume V have similarly sized non-sister neighboring cells on average $|(V - V^{ns\text{-}neigh})/(V + V^{ns\text{-}neigh})| \leq 0.11$, or differently sized non-sister neighboring cells $|(V - V^{ns\text{-}neigh})/(V + V^{ns\text{-}neigh})| > 0.11$.

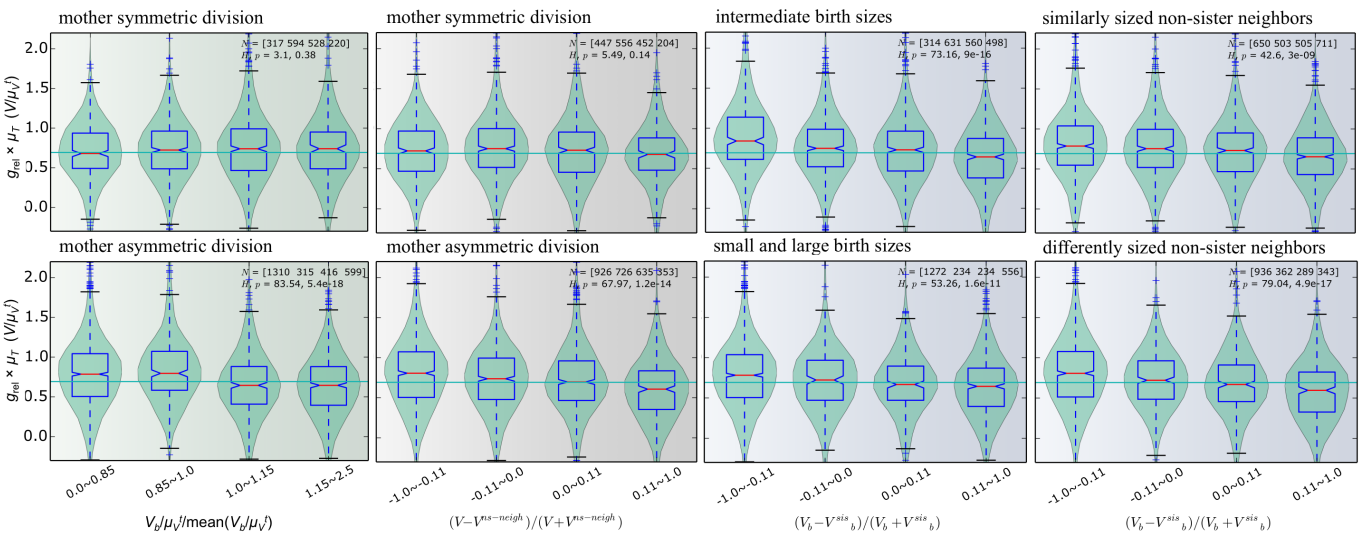

Fig. S20: Different relative growth rates between sisters result from asymmetric divisions of the mother cell. Cells generated by a symmetric division ($|\alpha_b| \leq 0.11$) grow at the same relative rate regardless of their birth volume (top row, left panel; Kruskal-Wallis $H = 3.1$, $p = 0.38$) or the relative size of their non-sister neighbors (top row, middle-left panel; Kruskal-Wallis $H = 5.5$, $p = 0.14$), while cells generated by asymmetric divisions have relative growth rates that depend on both birth volume and the relative size of their non-sister neighbors (bottom row, left and middle-left panel; Kruskal-Wallis $p < 10^{-13}$). The dependence of relative growth rate on mother-cell division asymmetry persists for cells born with intermediate volumes ($|V_b/\mu_V^t/\text{mean}(V_b/\mu_V^t) - 1| \leq 0.16$, top row, middle-right; Kruskal-Wallis $H = 73$, $p = 10^{-15}$) and for cells with non-sister neighbors of similar volumes ($|(V-V^{\text{ns-neigh}})/(V+V^{\text{ns-neigh}})| \leq 0.11$, top row, right; Kruskal-Wallis $H = 43$, $p = 10^{-9}$). The dependence also persists for cells born with excessively small or large volumes ($|V_b/\mu_V^t/\text{mean}(V_b/\mu_V^t) - 1| > 0.16$, bottom row, middle-right; Kruskal-Wallis $H = 53$, $p = 10^{-11}$) and cells with non-sister neighbors of significantly different relative sizes ($|(V-V^{\text{ns-neigh}})/(V+V^{\text{ns-neigh}})| > 0.11$, bottom row, right; Kruskal-Wallis $H = 79$, $p = 10^{-16}$). The data points included/excluded from each plot are presented in Fig. S19. In the upper right corner of each panel, the sample size N is

given for each violin, with left → right values corresponding to left → right violins. Together, these results indicate that differently sized sisters grow at different rates owing primarily to the asymmetric division of the mother cell, rather than to their being smaller/larger or their increased likelihood of neighboring comparatively smaller/larger cells.

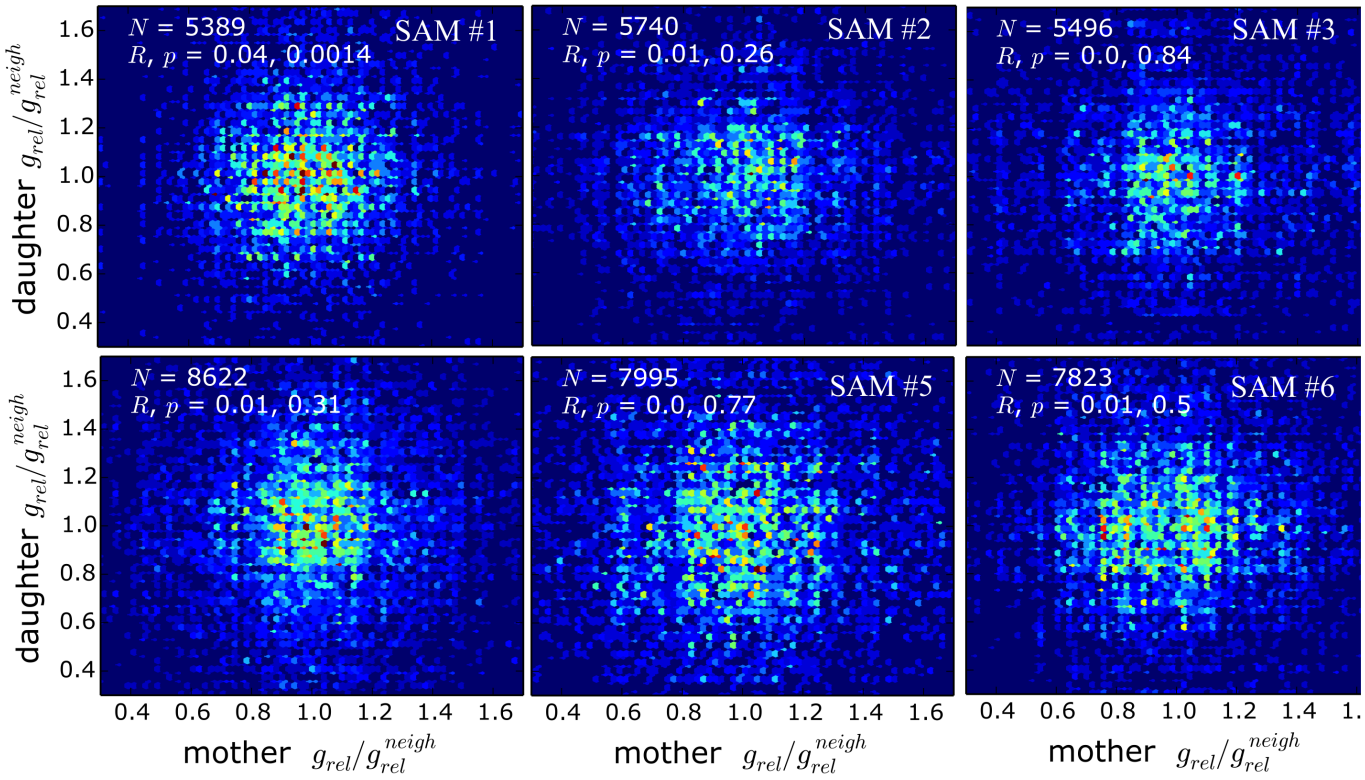

Fig. S21: Daughter relative growth rates are uncorrelated with mother relative growth rates. For the L1 central zone cells of each SAM, the volumetric relative growth rates of mother cells are not correlated with the volumetric relative growth rates of their progeny. Each cellular volumetric relative growth rate $g_{rel} = (V(t+\Delta t)-V(t))/\Delta t \times 2/(V(t+\Delta t)+V(t))$ was normalized by the mean relative growth rate of the neighboring cells, g_{rel}^{neigh}, to eliminate the correlation that would otherwise result purely as a consequence of the mother and daughter cells being located the same radial distance from *O*. In the heat map of each panel, red corresponds to high frequency and blue corresponds to low frequency.

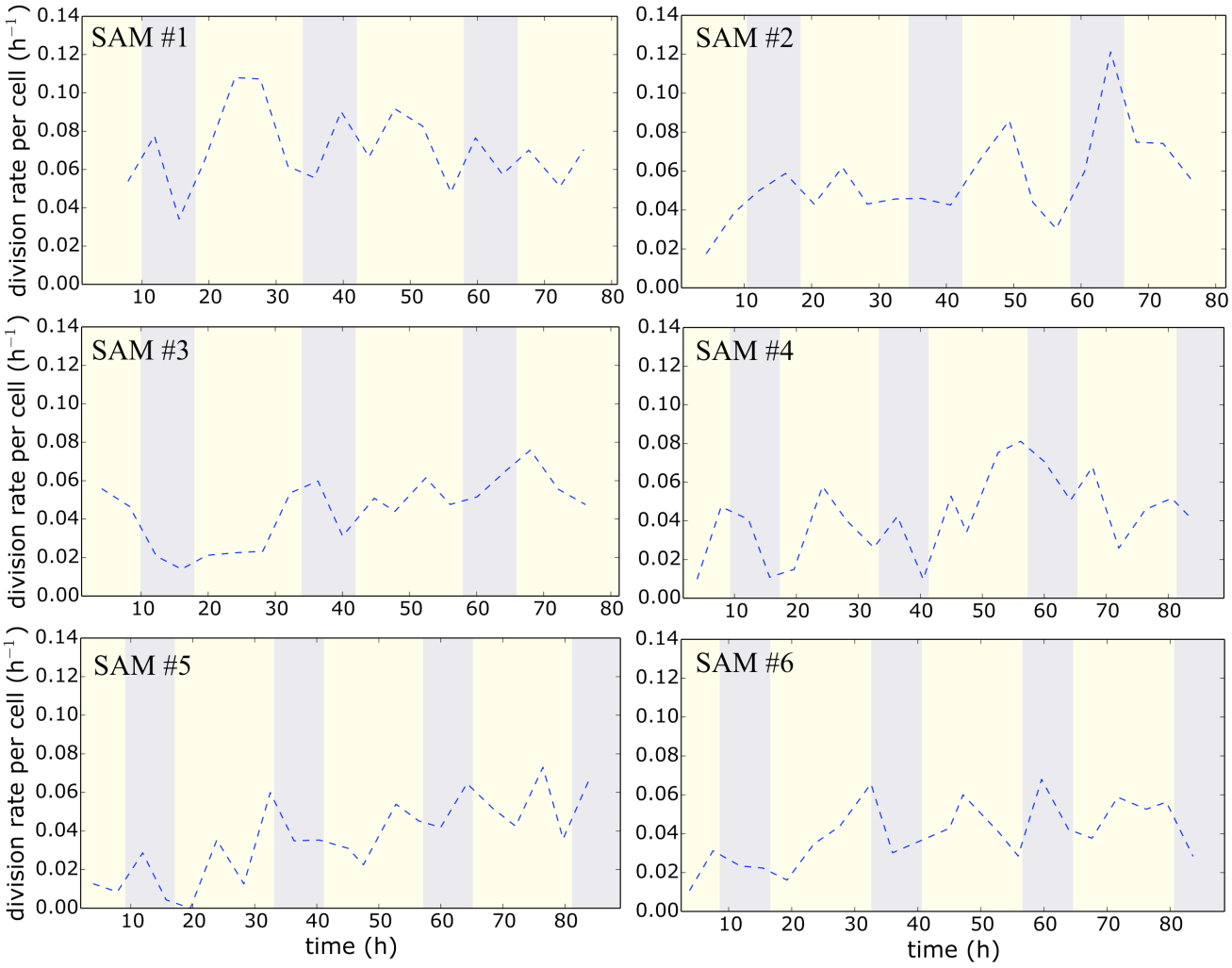

Fig. S22: There is no consistent discernible effect of light/dark cycles on the division rate. In each SAM, the division rate per cell varies over time throughout the time-lapse among the ~100 cells <30 μm from *O*, but there is no consistent discernible effect of light/dark cycles on the division rate (light/dark cycles shown by yellow/blue regions respectively). The higher division rate in SAM #1 may have been due to a small wound at the edge of the peripheral zone.

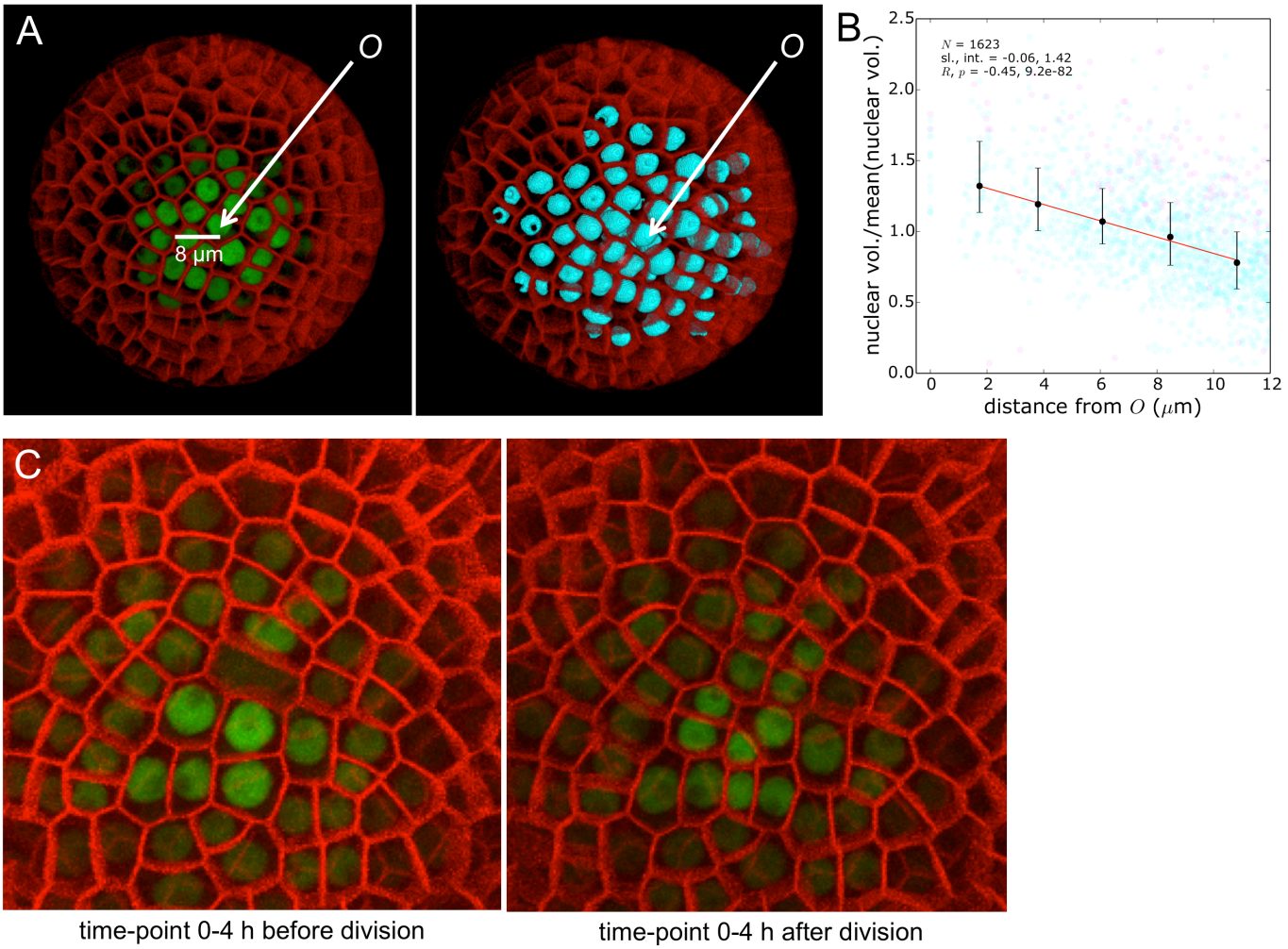

Fig. S23: Nuclear volume segmentations and quantification. (A-B) The nuclear-localized pCLV3::dsRED-N7 reporter permitted 6-9 nuclei, within a 3D Euclidean distance of 8 µm from the center of the SAM at *O,* to be accurately segmented (Materials and Methods). (A) The *CLAVATA3* (green) and membrane (red) reporters (left), and the corresponding nuclear segmentation (right). (B) The reduction in nuclear volume with distance from *O* is an artifact due to the effect of the decreasing *CLAVATA3* signal on the segmentations. Pink data points correspond to nuclei of cells that divide within the following ~0-4 h period. (C) The nuclear-localized *CLAVATA3* reporter was used to manually count the number of cell divisions in which the corresponding nuclei were diffuse in the preceding ~0-4 h; from this, the duration of mitosis

was estimated to be ≈40 min (Table S4). The panels show one example of a diffuse nucleus ~0-4 h prior to division. Segmentations of nuclei that are undergoing mitosis lead to computation of a nuclear volume that is close to zero (e.g. several pink data points in (B)).

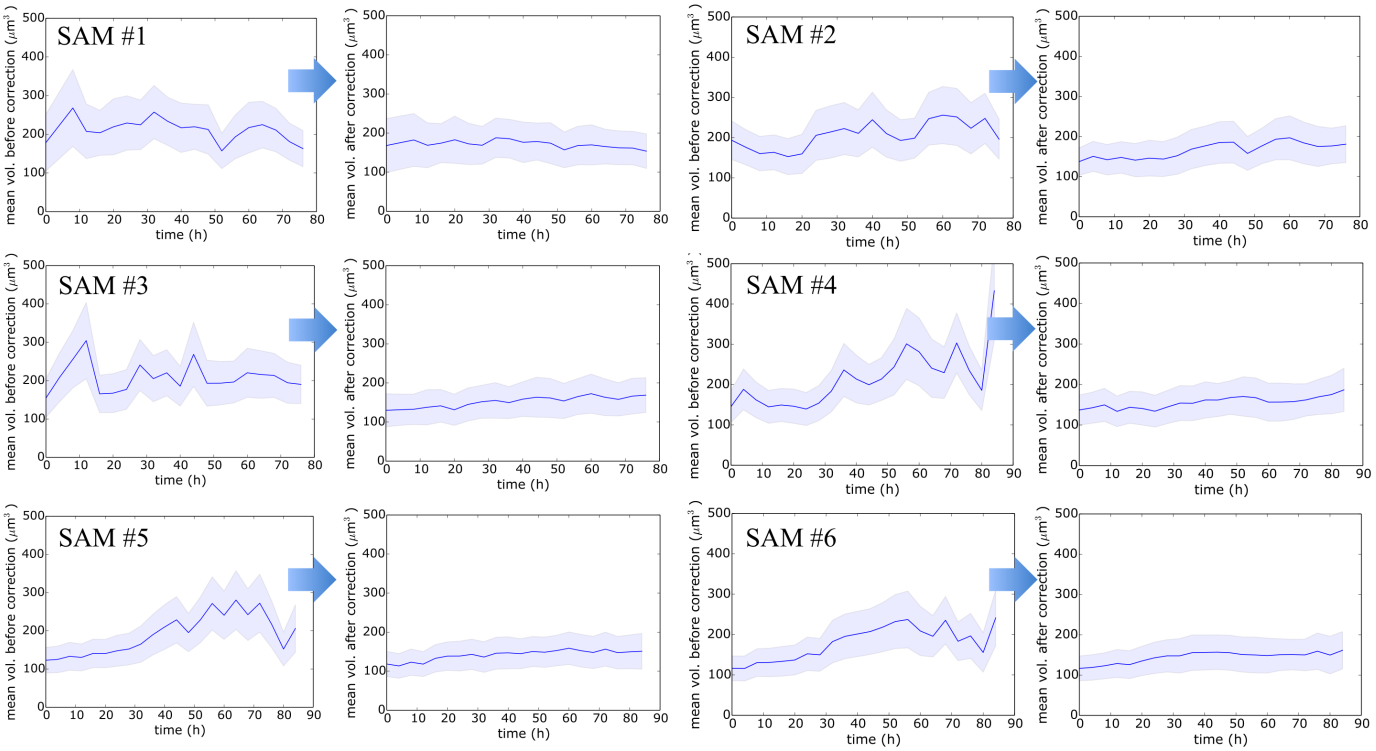

Fig. S24: The bias and noise in measurements of cell-size metrics from 3D segmentations of confocal *z*-stacks was strongly reduced by our method for correcting the artificial stretching of cells in the *z*-direction due to stem growth/SAM movement during time-lapse imaging (Materials and Methods). Compare the change in mean cell volume during the time-lapse before versus after the correction (left vs. right graphs for each SAM; blue lines enclosed by shaded regions represent mean volumes ± one standard deviation).

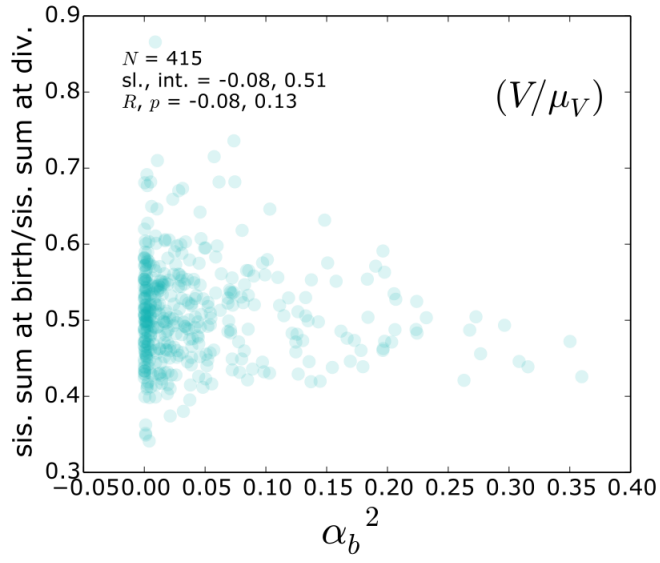
N = 415
sl., int. = -0.08, 0.51
R, p = -0.08, 0.13
(V/μ_V)
sis. sum at birth/sis. sum at div.
$\alpha_b{}^2$

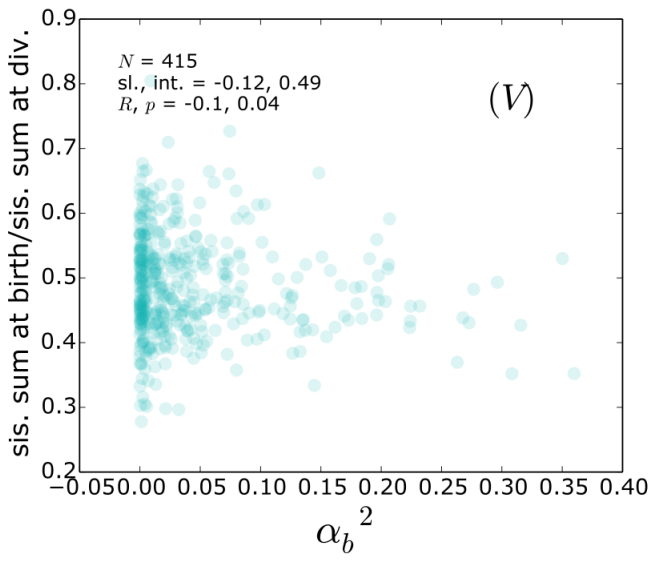
N = 415
sl., int. = -0.12, 0.49
R, p = -0.1, 0.04
(V)
sis. sum at birth/sis. sum at div.
$\alpha_b{}^2$

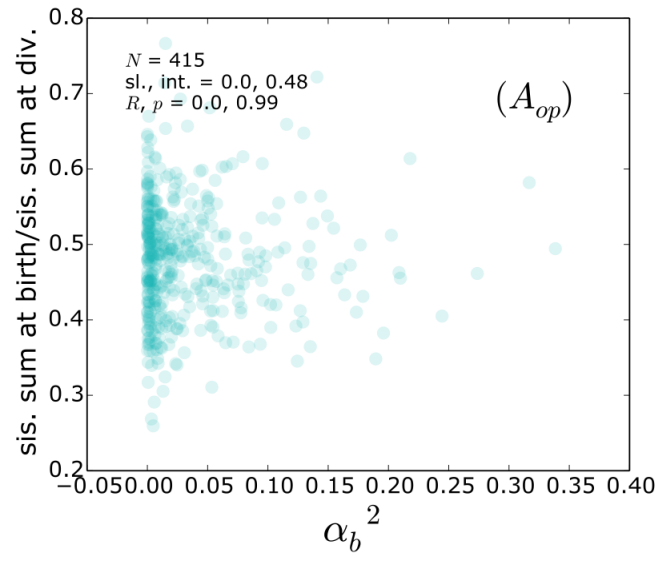
N = 415
sl., int. = 0.0, 0.48
R, p = 0.0, 0.99
(A_{op})
sis. sum at birth/sis. sum at div.
$\alpha_b{}^2$

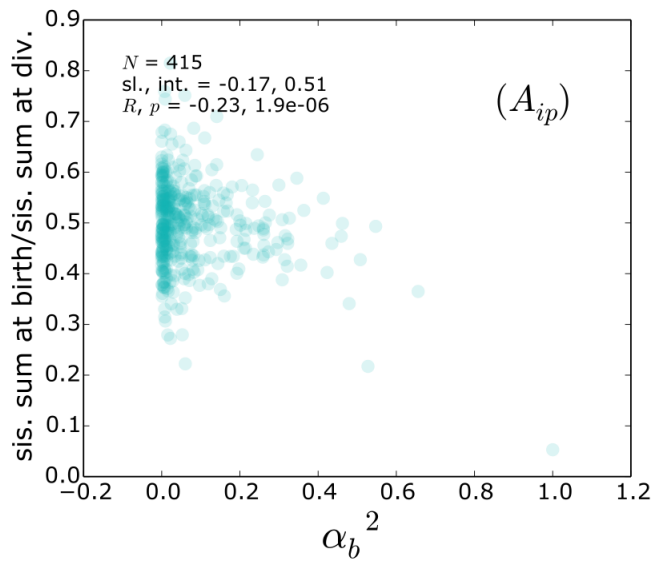
N = 415
sl., int. = -0.17, 0.51
R, p = -0.23, 1.9e-06
(A_{ip})
sis. sum at birth/sis. sum at div.
$\alpha_b{}^2$

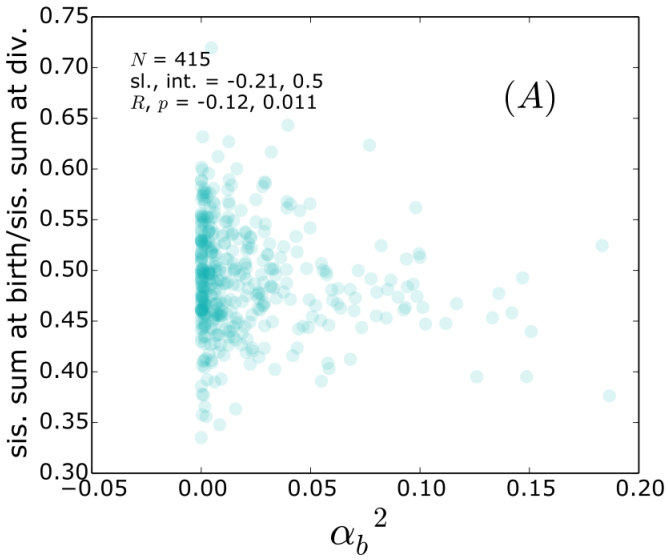
N = 415
sl., int. = -0.21, 0.5
R, p = -0.12, 0.011
(A)
sis. sum at birth/sis. sum at div.
$\alpha_b{}^2$

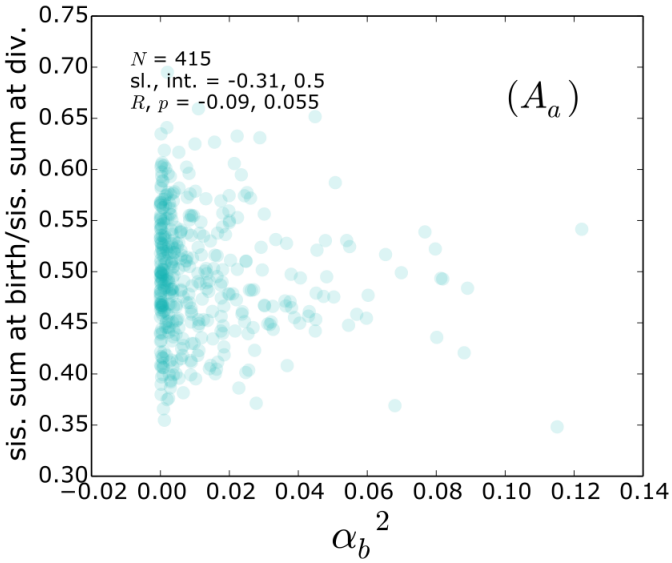
N = 415
sl., int. = -0.31, 0.5
R, p = -0.09, 0.055
(A_a)
sis. sum at birth/sis. sum at div.
$\alpha_b{}^2$

Fig. S25: The degree of asymmetric division, quantified by α_b^2, is uncorrelated with the ratio of the sum of sister-size metrics at birth versus division, $(S_b+S_b^{sis})/(S_d+S_d^{sis})$, for cell-size metrics normalized volume V/μ_V^t (upper left), volume V (upper right), outer periclinal wall area A_{op} (middle left), total wall area A (bottom left), and anticlinal wall area A_a (bottom right). The correlation between α_b^2 and inner periclinal wall area A_{ip} (middle right) is significant; however, examination of the corresponding plot suggests that this correlation is due to a single outlier.

Supplementary Tables:

Table S1: Cell-size distributions and cell-cycle statistics for SAMs #1-6. In all SAMs, the coefficient of variation of cell volumes (σ_V) is similar (~0.3), while the mean cell volume (μ_V) varies by 1.2-fold from 141 μm^3 to 171 μm^3 and the mean outer periclinal surface area (μ_{Aop}) of 35 μm^2. The mean inter-division time (μ_T) varies from 21 h to 31 h. Among all SAMs, the mean cell volume is 1.3-1.4x the mean cell birth volume. The coefficients of variation in volume at birth (σ_b), volume at division (σ_d), and asymmetric cell division (σ_a = standard deviation of $(V_b - V_b^{sis})/2(V_b + V_b^{sis})$) were highly consistent among the SAMs. Histograms of the number of neighbors in the L1 layer (N_{neigh}) were positively skewed, with a peak at $N_{neigh} = 6$ (Fig. S1). The time-averaged distribution of outer periclinal wall area was significantly non-normal with a positive skewness (Fig. S2). Slopes and intercepts from least-square linear fits of number of neighbors (N_{neigh}) vs. outer periclinal wall area (A_{op}) were consistent with Lewis's Law (32, 33).

	μ_V (μm^3)	μ_{Aop} (μm^2)	σ_V	V skew., p	μ_T (h)	μ_V/μ_b	σ_b	σ_d	σ_a	N_{neigh} vs. A_{op} slope, int.
#1	171	34	0.31	0.76, 10^{-34}	21	1.3	0.26	0.17	0.11	0.19, -0.16
#2	165	35	0.30	0.33, 10^{-9}	25	1.4	0.29	0.13	0.11	0.18, -0.10
#3	153	35	0.30	0.26, 10^{-5}	27	1.3	0.28	0.11	0.11	0.20, -0.22
#4	156	35	0.29	0.26, 10^{-6}	29	1.3	0.25	0.12	0.11	0.18, -0.11
#5	141	33	0.29	0.21, 10^{-5}	31	1.3	0.28	0.11	0.12	0.18, -0.19
#6	144	36	0.29	0.27, 10^{-6}	31	1.3	0.25	0.14	0.10	0.19, -0.12
Median	155	35	0.30	0.27	28	1.3	0.27	0.13	0.11	0.19, -0.14

Table S2: The degree of asymmetry between sister cells $|\alpha_b| = |(S_b - S^{sis}{}_b)/(S_b + S^{sis}{}_b)|$ for different cell-size metrics does not depend on Euclidean 3D distance from *O*, where distance is measured in units of (mean cell volume)$^{1/3}$. This lack of dependence is evident based on the slopes of least-square linear fits (sl.) to distance vs. $|\alpha_b|$ being close to zero and the corresponding absent or weak correlations; see also Fig. S10-S14. Similar relationships hold for $|\alpha_d| = |(S_d - S^{sis}{}_d)/(S_d + S^{sis}{}_d)|$. There was a weak dependence of $|\alpha_b|$ on time from the start of data acquisition; however, this correlation disappeared when 50% of data points, corresponding to cells born late in the time-lapse ($t > t_{med}$), are removed. Removing these data did not impact other statistics and therefore any of our conclusions (Table S6). Moreover, $|\alpha_T| = |(T - T^{sis})/(T + T^{sis})|$, where T is a cell's inter-division time and T^{sis} is the corresponding sister cell's inter-division time, did not depend on distance or time: for distance vs. $|\alpha_T|$, $R = 0.04$ and $p = 0.39$; for time vs. $|\alpha_T|$, $R = -0.1$ and $p = 0.04$. Our analysis includes all pairs of L1 sisters with complete cell cycles that began <45 μm from *O* ($N = 415$).

var.	distance vs. $\lvert\alpha_b\rvert$		distance vs. $\lvert\alpha_d\rvert$	
	sl., int.	R, p	sl., int.	R, p
V/μ_V^t	-0.01, 0.21	0.13, 0.01	0.00, 0.05	0.08, 0.09
V	-0.01, 0.21	-0.13, 0.01	0.00, 0.05	0.08, 0.09
A	-0.01, 0.14	-0.12, 0.02	0.00, 0.03	0.11, 0.03
A_{op}	-0.01, 0.17	-0.07, 0.2	0.01,0.05	0.15, 0.002
A_{ip}	0.00, 0.23	-0.04, 0.5	0.00, 0.07	0.07, 0.1
A_a	0.00, 0.10	-0.11, 0.03	0.00, 0.03	0.17, 0.0007

	time vs. $\lvert\alpha_b\rvert$		time vs. $\lvert\alpha_d\rvert$		time < t_{med} vs. $\lvert\alpha_b\rvert$		time < t_{med} vs. $\lvert\alpha_d\rvert$	
	sl., int.	R, p	sl., int.	R, p	sl., int.	R, p	sl., int.	R, p
V/μ_V^t	0.00, 0.21	-0.15, 0.002	0.00, 0.07	-0.03, 0.5	0.0, 0.21	-0.1, 0.2	0.0, 0.08	-0.15, 0.05
V	0.0, 0.21	-0.15, 0.002	0.00, 0.07	-0.03, 0.5	0.0, 0.21	-0.1, 0.2	0.0, 0.08	-0.15, 0.05
A	0.0, 0.14	-0.16, 0.001	0.00, 0.04	-0.01, 0.9	0.0, 0.14	-0.1, 0.15	0.0, 0.05	-0.12, 0.09
A_{op}	0.00, 0.18	-0.15, 0.002	0.00, 0.09	-0.15, 0.002	0.0, 0.18	-0.1, 0.15	0.0, 0.11	-0.19, 0.01
A_{ip}	0.00, 0.27	-0.16, 0.0009	0.00, 0.1	-0.12, 0.02	0.0, 0.29	-0.13, 0.08	0.0, 0.12	-0.12, 0.09
A_a	0.00, 0.11	-0.15, 0.003	0.00, 0.04	0.06, 0.2	0.0, 0.11	-0.11, 0.13	0.0, 0.04	0.02, 0.8

Table S3: Cell size statistics among L1 central zone cells tracked over ~3 generations indicate that neither division nor the G2/M transition are triggered when the cell reaches a critical volume or adds a critical volume increment (N =1013 cells). Normalized birth volume (V_b/μ_V^t) was positively correlated with normalized division volume (V_d/μ_V^t) and negatively correlated with normalized volume increment (Δ/μ_V^t). The results were similar for non-normalized birth and division volumes (V_b/μ_b and V_d/μ_b, where μ_b is the mean birth volume among all cells tracked through a complete cell cycle in each SAM). The slopes (sl.) and intercepts (int.) from least-square linear fits between variables are given, along with Pearson R correlation coefficients and corresponding p-values. The parameter f that characterizes the size regulation rule is estimated by the slopes of normalized birth size vs. normalized division size (see also Table S5). Outliers beyond 2.5 standard deviations (~3% of data) were removed for SAMs #1-6 but not for pooled data; removing these outliers does not significantly affect the correlations.

SAM	*N*	V_b/μ_V^t vs V_d/μ_V^t		V_b/μ_V^t vs Δ/μ_V^t	
		sl., int.	*R*, *p*	sl., int.	*R*, *p*
#1	296	0.48, 1.2	0.47, 10^{-17}	-0.52, 1.2	-0.50, 10^{-20}
#2	183	0.36, 1.3	0.37, 10^{-7}	-0.64, 1.3	-0.58, 10^{-17}
#3	113	0.45, 1.2	0.53, 10^{-9}	-0.55, 1.2	-0.61, 10^{-12}
#4	154	0.57, 1.0	0.59, 10^{-15}	-0.43, 1.0	-0.48, 10^{-10}
#5	100	0.35, 1.2	0.44, 10^{-5}	-0.65, 1.2	-0.67, 10^{-14}
#6	122	0.50, 1.1	0.49, 10^{-8}	-0.50, 1.1	-0.50, 10^{-9}
pooled data	1013	0.48, 1.2	0.47, 10^{-56}	-0.52, 1.2	-0.50, 10^{-64}
	N	V_b/μ_b vs V_d/μ_b		V_b/μ_b vs Δ/μ_b	
		sl., int.	*R*, *p*	sl., int.	*R*, *p*
#1	296	0.48, 1.4	0.46, 10^{-16}	-0.52, 1.4	-0.49, 10^{-19}
#2	183	0.37, 1.9	0.40, 10^{-8}	-0.63, 1.85	-0.60, 10^{-18}
#3	113	0.43, 1.7	0.50, 10^{-8}	-0.57, 1.7	-0.61, 10^{-13}
#4	154	0.53, 1.5	0.54, 10^{-12}	-0.47, 1.5	-0.50, 10^{-10}
#5	100	0.32, 1.6	0.41, 10^{-5}	-0.68, 1.6	-0.69, 10^{-15}
#6	122	0.41, 1.6	0.50, 10^{-6}	-0.59, 1.6	-0.55, 10^{-10}
pooled data	1013	0.45, 1.5	0.40, 10^{-41}	-0.55, 1.5	-0.48, 10^{-58}

Table S4: Mitosis and subsequent formation of the new membrane/cell wall took place over ≈40 min. The nuclear-localized pCLV3::dsRED-N7 signal enabled clear visualization of cell nuclei within 10 μm of the SAM's center at *O*. Within this region, we manually counted the number of cell divisions for which the nuclei appeared diffuse (Fig. S23C), and therefore were undergoing mitosis, in the confocal *z*-stack acquired between 0 and ~4 h prior to each division. Using this data, we estimated the duration of M-phase as (number of divisions with diffuse nuclei)/(total number of divisions) × 4 h = 13/80 × 4 h = 0.65 h ≈ 40 min. pCLV3::dsRED-N7 was not expressed in SAM #1.

SAM	total num. divisions <10 μm from *O*	num. divisions with diffuse nuclei <10 μm from *O*
#2	16	2
#3	16	2
#4	17	4
#5	18	1
#6	13	4
Total	80	13

Table S5: Cell-cycle statistics of L1 sister cells indicate that there is neither a critical size nor a critical increment checkpoint that triggers division or G2/M. Asymmetry between sister-cell sizes (N = 415 sister pairs) at birth, $\alpha_b = (S_b - S_b^{sis})/(S_b + S_b^{sis})$ for e.g. $S = V$ corresponding to volume, correlates strongly with division asymmetry, $\alpha_d = (S_d - S_d^{sis})/(S_d + S_d^{sis})$, and asymmetry in sister-size increments, $\alpha_\Delta = (\Delta - \Delta^{sis})/(\Delta + \Delta^{sis})$. These statistics are independent of a cell's position in the SAM and the time at which the data point was collected (Table S6). The medians and means of the ratios $(S_b + S_b^{sis})/(S_d + S_d^{sis}) \approx 0.5$ and $(S_b + S_b^{sis})/(\Delta + \Delta^{sis}) \approx 1$ indicate that, for each size metric, on average across the sample cells double in size over the cell cycle. These means and the slopes fitted to α_b vs. α_d and α_b vs. α_Δ were together used to estimate f, the parameter characterizing the mode of cell size regulation (*SI Appendix*, *Text S3*). The analysis includes all sisters born within 45 μm of O.

var.	med., mean $(S_b + S_b^{sis})/(S_d + S_d^{sis})$	med., mean $(S_b + S_b^{sis})/(\Delta + \Delta^{sis})$	α_b vs. α_d			α_b vs. α_Δ			α_b vs. α_T	
			sl., int.	R, p	est. f	sl,, int.	R, p	est. f	sl., int.	R, p
V/μ_V^t	0.50, 0.50	1.01, 1.08	0.23, 0.0	0.61, 10^{-43}	0.46	-0.55, 0.0	-0.64, 10^{-48}	0.45	-0.71, 0.0	-0.82, 10^{-103}
V	0.48, 0.49	0.92, 1.00	0.23, 0.0	0.61, 10^{-42}	0.46	-0.48, 0.0	-0.59, 10^{-40}	0.52	-0.71, 0.0	-0.82, 10^{-103}
A	0.49, 0.49	0.95, 0.99	0.21, 0.0	0.55, 10^{-34}	0.42	-0.52, 0.0	-0.62, 10^{-45}	0.48	-1.03, 0.0	-0.82, 10^{-102}
A_{op}	0.48, 0.48	0.93, 0.97	0.23, 0.0	0.46, 10^{-22}	0.46	-0.48, 0.0	-0.48, 10^{-25}	0.52	-0.74, 0.0	-0.77, 10^{-82}
A_{ip}	0.50, 0.50	0.99, 1.05	0.29, 0.0	0.69, 10^{-61}	0.58	-0.39, 0.0	-0.52, 10^{-29}	0.61	-0.48, 0.0	-0.72, 10^{-67}
$A_{a,}$	0.49, 0.49	0.97, 1.01	0.21, 0.0	0.55, 10^{-34}	0.42	-0.50, 0.0	-0.47, 10^{-23}	0.50	-1.3, 0.0	-0.79, 10^{-91}

Table S6: Cell-cycle statistics from volumes of all sister cells born within 45 μm of *O* (*N* = 415 sister pairs) are robust when the data were split for each SAM into the following categories: random splitting; cells born in the first/second half of the experiment (early times/late times); cells born closer/farther than the median distance from *O* (central zone/peripheral zone); cells born with larger/smaller volume than the median of L1 neighboring cells (large/small neighbor volume); cells born in the first 0-8 h light period/8-16 h light period/8 h dark period (born in morning/afternoon/dark); cells with a mother volume upon division that is larger/smaller than the median; cells born from symmetric/asymmetric divisions with $|\alpha_b| \leq 0.11$ or $|\alpha_b| > 0.11$. Statistics from all cells born within 30 μm of *O* (*N* = 1013 cells) pertaining to normalized birth volume versus normalized division volume (V_b/μ_V^t vs. V_d/μ_V^t) were robust when the data were split for each SAM into the following categories: cells born closer/farther than the median distance from *O* of cells within the 30-μm radius (inner central zone/outer central zone); cells born closer/farther than a 15-μm radius; cells born smaller/larger than the median birth volume; cells born with 5 or less/7 or more neighbors in the epidermal L1 cell layer; cells that divide with 5 or less/7 or more neighbors in the epidermal L1 cell layer; cells born in the first/second half of the experiment (early times/late times).

Data set split according to:	N	α_b vs. α_Δ (<45 μm)			α_b vs. α_T (<45 μm)	
		sl,, int.	R, p	est. f	sl., int.	R, p
random	222	-0.45, 0.0	-0.56, 10^{-19}	0.55	-0.68, 0.0	-0.79,.10^{-49}
early times	189	-0.44, 0.0	-0.38, 10^{-8}	0.56	-0.67, 0.0	-0.78, 10^{-40}
late times	226	-0.51, 0.0	-0.6, 10^{-23}	0.49	-0.73, 0.0	-0.82, 10^{-56}
central zone (for 45-μm radius)	207	-0.50, 0.0	-0.67, 10^{-30}	0.50	-0.68, 0.0	-0.86, 10^{-61}
peripheral zone (for 45-μm radius)	208	-0.46, 0.0	-0.52, 10^{-15}	0.54	-0.73, 0.0	-0.79, 10^{-45}
large neighbor vol.	208	-0.45, 0.0	-0.54, 10^{-17}	0.55	-0.72, 0.0	-0.78, 10^{-44}
small neighbor vol.	207	-0.51, 0.0	-0.64, 10^{-25}	0.49	-0.70, 0.0	-0.86, 10^{-63}
born in morning	140	-0.39, 0.0	-0.59, 10^{-14}	0.61	-0.68, 0.0	-0.68, 10^{-34}
born in afternoon	148	-0.54, 0.0	-0.6, 10^{-16}	0.46	-0.71, 0.0	-0.81, 10^{-35}
born in dark	127	-0.51, 0.0	-0.59, 10^{-13}	0.49	-0.73, 0.0	-0.84, 10^{-34}
large mother vol.	208	-0.5, 0.0	-0.54, 10^{-16}	0.50	-0.74, 0.0	-0.81, 10^{-48}
small mother vol.	207	-0.47, 0.0	-0.66, 10^{-26}	0.53	-0.68, 0.0	-0.84, 10^{-56}
symmetric birth	174	-0.58, 0.0	-0.23, 10^{-3}	0.42	-0.85, 0.0	-0.44, 10^{-9}
asymmetric birth	241	-0.48, 0.0	-0.69, 10^{-35}	0.52	-0.7, 0.0	-0.88, 10^{-77}
	N	V_b/μ_V^t vs. V_d/μ_V^t (< 30 μm)		N	V_b/μ_b vs. V_d/μ_b (< 30 μm)	
		sl,, int.	R, p		sl,, int.	R, p
inner central zone (split 50:50 for 30-μm radius)	505	0.45, 1.2	0.52, 10^{-36}	505	0.44, 1.6	0.55, 10^{-26}
outer central zone (split 50:50 for 30-μm radius)	508	0.51, 1.1	0.44, 10^{-25}	508	0.44, 1.5	0.36, 10^{-17}
inner central zone (for 15-μm radius)	190	0.45, 1.2	0.6, 10^{-19}	190	0.43, 1.6	0.49, 10^{-13}
outer central zone (for 15-μm radius)	823	0.49, 1.2	0.45, 10^{-42}	823	0.46, 1.5	0.39, 10^{-31}
large birth vol.	508	0.63, 1.0	0.45, 10^{-26}	508	0.66, 1.1	0.42, 10^{-22}

small birth vol.	505	0.49, 1.2	0.32, 10^{-13}	505	0.42, 2.0	0.20, 10^{-6}
num. neighbors at birth ≤ 5	383	0.43, 1.2	0.34, 10^{-11}	383	0.39, 2.0	0.27, 10^{-7}
num. neighbors at birth ≥ 7	183	0.59, 1.0	0.47, 10^{-11}	183	0.63, 1.0	0.47, 10^{-11}
num. neighbors at division ≤ 6	346	0.54, 1.1	0.46, 10^{-19}	346	0.45, 1.5	0.34, 10^{-10}
num. neighbors at division ≥ 8	191	0.47, 1.2	0.53, 10^{-15}	191	0.49, 1.5	0.47, 10^{-11}
early times	439	0.52, 1.2	0.50, 10^{-28}	439	0.49, 1.7	0.38, 10^{-16}
late times	574	0.47. 1.1	0.47, 10^{-32}	574	0.48. 1.36	0.46, 10^{-30}

Table S7: The power-law scalings of volume with inner periclinal wall area and anticlinal wall area are $V \sim A_{ip}$ and $V \sim A_a^{0.5}$, as expected for L1 cells in the central zone given that these cells grow within the plane of the epidermis. The outer periclinal wall area scaled with volume like $V \sim A_{op}^{0.8}$ and the total wall area scaled like $V \sim A^{0.66}$. Each entry displays the least-square linear fitted slope (Pearson's R, p).

SAM	log(V) vs. log(A)	log(V) vs. log(A_a)	log(V) vs. log(A_{ip})	log(V) vs. log(A_{op})
#1	0.67 (0.99, 0.0)	0.52 (0.92, 0.0)	1.03 (0.85, 0.0)	0.77 (0.75, 0.0)
#2	0.66 (0.99, 0.0)	0.55 (0.91, 0.0)	0.98 (0.89, 0.0)	0.79 (0.88, 0.0)
#3	0.66 (1.0,0.0)	0.51 (0.91, 0.0)	1.02 (0.92, 0.0)	0.82 (0.9, 0.0)
#4	0.67 (0.99, 0.0)	0.53 (0.9, 0.0)	0.98 (0.89, 0.0)	0.82 (0.82, 0.0)
#5	0.66 (0.99, 0.0)	0.51 (0.85, 0.0)	1.0 (0.88, 0.0)	0.88 (0.82, 0.0)
#6	0.67 (1.0, 0.0)	0.53 (0.86, 0.0)	0.88 (0.88, 0.0)	0.85 (0.89, 0.0)

Table S8: Sister cells generated by an asymmetric division grow at different relative rates with the smaller cell growing at a faster relative rate. Left two columns: the proportion of the size metric *S* inherited from the mother cell upon division, quantified by the value of $\alpha_b = (S_b - S_b^{sis})/(S_b + S_b^{sis})$ at birth, is strongly negatively correlated with the relative growth rate g_{rel} divided by its mean (α_b vs. $g_{rel}/\text{mean}(g_{rel})$). If sisters grew at the same relative rate, there would be no correlation. Right four columns: among cells born from a symmetric division (similar volumes between sisters; $|(V_b - V_b^{sis})/(V_b + V_b^{sis})| \leq 0.11$, representing ~50% of data), for all size metrics there was no significant dependence of relative growth rate on either cell birth volume ($p > 0.01$) or the relative volume of their non-sister neighbors ($p > 0.01$). In contrast, for cells of intermediate birth volumes ($|V_b/\text{mean}(V_b) - 1| \leq 0.16$, representing ~50% of the data) and with non-sister neighbors of a similar volume ($|(V - V^{ns\text{-}neigh})/(V + V^{ns\text{-}neigh})| \leq 0.11$, representing ~50% of the data), the relative growth rates of volume, outer periclinal, and inner periclinal wall areas did depend on mother-cell asymmetric division (Fig. S20). Data points include relative growth rates for all cells born <30 μm from *O* ($N = 393$ sister pairs).

	α_b vs. g_{rel}/mean(g_{rel})		Kruskal-Wallis H-test (H, p) for g_{rel} for the given size metric and group			
			~50% data with symmetric division of mother cell		grouped by asymmetric division of mother cell	
var. S	sl., int.	R, p	grouped by cell vol. at birth	grouped by non-sister neighbor vols.	~50% data with intermediate vols. at birth	~50% data with vols. similar to non-sister neighbors
V/μ_V^t	-0.50, 0.99	-0.36, 10^{-24}	3.1, 0.4	5.5, 0.1	73, 10^{-15}	43, 10^{-9}
V	-0.34, 0.99	-0.30, 10^{-17}	4.6, 0.2	8.5, 0.04	18, 4.10^{-4}	12, 6.10^{-3}
A	-0.45, 0.98	-0.26, 10^{-13}	3.7, 0.3	4.2, 0.2	8.9, 0.03	8.0, 0.04
A_{op}	-0.38, 0.99	-0.25, 10^{-12}	14, 0.003	9.4, 0.02	49, 10^{-10}	49, 10^{-10}
A_{ip}	-0.56, 0.98	-0.19, 10^{-7}	2.4, 0.5	7.0, 0.07	51, 10^{-10}	58, 10^{-12}
A_a	-0.53, 1.0	-0.16, 10^{-5}	3.0, 0.4	7.6, 0.06	1.1, 0.8	0.81, 0.9

Table S9: Simulations of cell-autonomous size and growth regulation recapitulate statistics. Simulations of n_{model} cell cycles, where n_{model} was chosen to approximately match the sample size of our data, assuming cell-autonomous regulation of division size according to Eq. (1) and growth at a constant relative rate over the cell cycle that depended linearly on the fraction of volume inherited from the mother cell at birth. 1000 instances of the simulation were used to compute median values of various statistics and 90% confidence intervals. Simulation parameters were extracted from experimental data (f = 0.48, g_{asym} = 0.43, σ = 0.227, σ_a = 0.105, correspond to medians computed by bootstrapping; *SI Appendix*, *Text S3*). The experimental least-square linear fitted slopes (sl.), intercepts (int.), Pearson correlation coefficients (R), and p-values (p) were also estimated by medians from bootstrapping. There are no free fitting parameters, and the simulation predictions are in close agreement with our experimental data.

	σ_b, σ_d	normalized vol.: V_b/μ_V^t vs. V_d/μ_V^t/mean(V_b/μ_V^t) (n_{model} = 1000)	
		sl., int.	*R*, *p*
simulation	(0.25, [0.24, 0.26]), (0.13, [0.12, 0.13])	(0.48, [0.43,0.53]), (1.52, [1.47,1.57])	(0.47, [0.42, 0.51]), (10^{-56}, [10^{-53}, 10^{-34}])
experiments	0.25, 0.13	0.48, 1.43	0.47, 10^{-57}
		α_b vs. α_d (n_{model} = 800)	
		sl,, int.	*R*, *p*
simulation		(0.24, [0.21,0.27]), (0.00, [0.00, 0.00])	(0.53, [0.48, 0.58]), (10^{-30}, [10^{-37}, 10^{-23}])
experiments		0.23, 0.00	0.61, 10^{-43}
		α_b vs. α_T (n_{model} = 800)	
		sl., int.	*R*, *p*
simulation		(-0.69, [-0.75,-0.65]), (0.0, [-0.01,0.01])	(-0.75, [-0.78,-0.70]), (10^{-72}, [10^{-82},10^{-61}])
experiments		-0.71, 0.0	-0.82, 10^{-102}
		normalized vol.: α_b vs. V_b/μ_V^t/mean(V_b/μ_V^t) (n_{model} = 800)	
		sl., int.	*R*, *p*
simulation		(1.00, [0.95,1.05]), (1.00, [0.99, 1.01])	(0.85, [0.82,0.87]), (10^{-120}, [10^{-125},10^{-100}])
experiments		0.99, 1.00	0.87, 10^{-245}

Table S10. Correction factors strongly reduce the bias and noise in measurements of cell-size metrics. Bias and noise resulted from plant stem growth/upward movement of SAMs during image acquisition, which produced artificial stretching of cells in the *z*-direction by the factor given in the table for each time-point; see also Fig. S24. Correction factors were computed by comparing rapidly acquired low-*z*-resolution confocal stacks with slowly acquired high-*z*-resolution confocal stacks, with the latter being used for segmentation (Materials and Methods).

Time-point (h)	SAM #1	SAM #2	SAM #3	SAM #4	SAM #5	SAM #6
0	1.07	1.41	1.19	1.06	1.04	1.00
4	2.77	1.17	1.58	1.32	1.11	0.98
8	1.47	1.13	1.93	1.08	1.08	1.06
12	1.23	1.10	2.21	1.08	1.11	1.02
16	1.17	1.08	1.17	1.04	1.06	1.06
20	1.20	1.09	1.27	1.04	1.01	1.01
24	1.33	1.43	1.22	1.04	1.07	1.07
28	1.33	1.40	1.59	1.07	1.07	1.01
32	1.37	1.32	1.32	1.19	1.21	1.24
36	1.26	1.19	1.47	1.54	1.30	1.26
40	1.23	1.32	1.17	1.32	1.43	1.28
44	1.23	1.13	1.64	1.24	1.58	1.32
48	1.22	1.22	1.20	1.28	1.30	1.40
52	1.00	1.13	1.26	1.43	1.54	1.54
56	1.15	1.28	1.19	1.80	1.78	1.58
60	1.28	1.30	1.28	1.80	1.52	1.41
64	1.36	1.37	1.32	1.53	1.84	1.30
68	1.30	1.27	1.35	1.46	1.64	1.56
72	1.12	1.40	1.17	1.87	1.74	1.22
76	1.06	1.08	1.13	1.39	1.47	1.24
80				1.06	1.02	1.04
84				2.32	1.37	1.50

Other Supplemental Material:

External Database S1. The processed confocal *z*-stacks, segmented *z*-stacks, and cell quantification and tracking data files can be downloaded from Cambridge University D-space Repository (https://www.repository.cam.ac.uk/).